



JGR Biogeosciences

RESEARCH ARTICLE

10.1029/2019JG005428

Key Points:

- A process-based biogeochemistry model was revised, parameterized, and verified for various wetland ecosystems across the globe
- Methane fluxes and model uncertainties were quantified in global scale during 1950–2012
- More in situ methane flux data, more accurate wetland type, and area distribution information are needed

Supporting Information:

- Supporting Information S1

Correspondence to:

Q. Zhuang,
qzhuang@purdue.edu

Citation:

Liu, L., Zhuang, Q., Oh, Y., Shurpali, N. J., Kim, S., & Poulter, B. (2020). Uncertainty quantification of global net methane emissions from terrestrial ecosystems using a mechanistically based biogeochemistry model. *Journal of Geophysical Research: Biogeosciences*, 125, e2019JG005428. <https://doi.org/10.1029/2019JG005428>

Received 16 AUG 2019

Accepted 5 MAY 2020

Accepted article online 11 MAY 2020

Author Contributions:

Conceptualization: Licheng Liu, Qianlai Zhuang

Data curation: Licheng Liu, Qianlai Zhuang, Narasinha J. Shurpali, Ben Poulter

Formal analysis: Licheng Liu

Funding acquisition: Qianlai Zhuang

Investigation: Licheng Liu, Qianlai Zhuang, Youmi Oh, Narasinha J. Shurpali, Ben Poulter

Methodology: Licheng Liu, Qianlai Zhuang, Youmi Oh, Ben Poulter

Project administration: Qianlai Zhuang

Resources: Licheng Liu, Qianlai Zhuang, Youmi Oh, Narasinha J. Shurpali, Ben Poulter

Software: Licheng Liu, Youmi Oh

Supervision: Qianlai Zhuang

Validation: Licheng Liu

(continued)

Uncertainty Quantification of Global Net Methane Emissions From Terrestrial Ecosystems Using a Mechanistically Based Biogeochemistry Model

Licheng Liu¹, Qianlai Zhuang^{1,2,3} , Youmi Oh¹, Narasinha J. Shurpali⁴ , Seungbum Kim⁵ , and Ben Poulter^{6,7} 

¹Department of Earth, Atmospheric, Planetary Sciences, Purdue University, West Lafayette, IN, USA, ²Department of Agronomy, Purdue University, West Lafayette, IN, USA, ³Purdue Climate Change Research Center, West Lafayette, IN, USA, ⁴Department of Environmental Science, University of Eastern Finland, Kuopio, Finland, ⁵Jet Propulsion Laboratory, California Institute of Technology, Pasadena, CA, USA, ⁶Department of Ecology, Montana State University, Bozeman, MT, USA, ⁷Biospheric Sciences Laboratory, NASA Goddard Space Flight Center, Greenbelt, MD, USA

Abstract Quantification of methane (CH_4) emissions from wetlands and its sinks from uplands is still fraught with large uncertainties. Here, a methane biogeochemistry model was revised, parameterized, and verified for various wetland ecosystems across the globe. The model was then extrapolated to the global scale to quantify the uncertainty induced from four different types of uncertainty sources including parameterization, wetland type distribution, wetland area distribution, and meteorological input. We found that global wetland emissions are 212 ± 62 and 212 ± 32 Tg CH_4 year $^{-1}$ ($1\text{Tg} = 10^{12}\text{ g}$) due to uncertain parameters and wetland type distribution, respectively, during 2000–2012. Using two wetland distribution data sets and three sets of climate data, the model simulations indicated that the global wetland emissions range from 186 to 212 CH_4 year $^{-1}$ for the same period. The parameters were the most significant uncertainty source. After combining the global methane consumption in the range of -34 to -46 Tg CH_4 year $^{-1}$, we estimated that the global net land methane emissions are 149 – 176 Tg CH_4 year $^{-1}$ due to uncertain wetland distribution and meteorological input. Spatially, the northeast United States and Amazon were two hotspots of methane emission, while consumption hotspots were in the Eastern United States and eastern China. During 1950–2016, both wetland emissions and upland consumption increased during El Niño events and decreased during La Niña events. This study highlights the need for more in situ methane flux data, more accurate wetland type, and area distribution information to better constrain the model uncertainty.

1. Introduction

Methane (CH_4) is the second most powerful greenhouse gas behind CO_2 and has contributed to about 20% of the observed warming since preindustrial times (Ciais et al., 2013). Atmospheric CH_4 concentrations have risen from preindustrial levels of 715 parts per billion (ppb) since the 1800s (Etheridge et al., 1998; MacFarling Meure et al., 2006) to over 1,800 ppb at the present. The growth rate of atmospheric CH_4 has decreased, however, from approximately 13 ppb year $^{-1}$ during the early 1980s to near zero between 1999 and 2006. Since 2007, the growth rate of atmospheric CH_4 has risen again (Dlugokencky et al., 2009; Nisbet et al., 2014; Saunois et al., 2016; Schaefer et al., 2016; Zhang et al., 2018). The interannual variability of atmospheric CH_4 is strongly related to the climatic sensitivity of biogenic CH_4 sources, of which global wetland CH_4 contributes 60–80% of natural emissions (Hopcroft et al., 2017; Quiquet et al., 2015) and this large role is likely to persist into the future (Zhang et al., 2017). Wetlands are an important component of the earth system and play a vital role in the global CH_4 cycling (Ciais et al., 2013; Zhang et al., 2002; Zhuang et al., 2004). CH_4 emissions from natural wetlands are the main drivers of the global interannual variability of CH_4 emissions with high confidence and contribute largely to interannual variations and anomalies of atmospheric CH_4 concentrations (Ciais et al., 2013; Zhuang et al., 2004). Therefore, it is important to improve existing CH_4 emission quantifications to better understand the role of global CH_4 cycling in the global climate system (Chen et al., 2013; Kirschke et al., 2013; Nisbet et al., 2014; Zhu et al., 2014; Zhuang et al., 2004).

To date, three approaches have been used in estimating CH_4 emissions from wetlands across different scales over the last few decades: (1) an extrapolation of flux measurements approach, which uses actual CH_4

Visualization: Licheng Liu

Writing - original draft: Licheng Liu

Writing - review & editing: Licheng Liu, Qianlai Zhuang, Youmi Oh, Narasinha J. Shurpali, Ben Poulter

emission measurements to scale up to global wetlands; (2) a bottom-up approach, which uses process-based models to quantify CH₄ fluxes; and (3) a top-down approach, which uses atmospheric inverse models to estimate the distribution of CH₄ sources and sinks by incorporating atmospheric observations, an atmospheric transport model, and prior estimates of source distributions and magnitudes (Anderson et al., 2010; Arneth et al., 2010; Kirschke et al., 2013; Zhu et al., 2014). Although top-down approach is widely thought to be more accurate than bottom-up approach, the current top-down approach may inadvertently include some incomplete observations and error amplifications during inverse modeling processes (Chen & Prinn, 2005; Ciais et al., 2013).

Process-based models can be used to improve CH₄ emission estimation considering the effects of complex interactions between soil, vegetation, and hydrology on CH₄ production and consumption processes. Process-based modeling became a practical alternative approach to scaling up site-level observation to regional or global scales (Cao et al., 1996; Li, 2000; Zhang et al., 2002; Zhuang et al., 2004). To date, a number of process-based models have been developed. Each has its own ways to implement wetland system complexity and CH₄ flux processes (Li, 2000; Meng et al., 2012; Walter & Heimann, 2000; Zhu et al., 2014; Zhuang et al., 2004). For instance, Cao et al. (1995, 1996) developed a CH₄ emission model for rice paddies based on C substrate level, soil organic matter (SOM) degradation, and environmental control factors and improved it for global natural wetland simulation; but the model has no specific CH₄ emission process. Walter and Heimann (2000) and Walter et al. (2001a, 2001b) developed a 1-D process-based climate sensitive model to estimate global long-term CH₄ emissions from natural wetlands, forced with net primary production derived from a separate model. Li (2000) developed a denitrification-decomposition model (DNDC) to simulate CH₄ emissions but only for rice paddies. Later, Zhang et al. (2002) adopted the DNDC model and some of its key components to simulate wetland ecosystem emissions. A process model (PEATLAND) was developed to simulate CH₄ flux from peat soils (van Huissteden et al., 2006) and upscaled for boreal and Arctic wetland simulations (Petrescu et al., 2010), although the model did not include explicit soil biogeochemical processes. Wania et al. (2010) integrated a CH₄ emission module into the modified dynamic global vegetation model Lund-Potsdam-Jena (LPJ) to simulate CH₄ emissions from northern peatlands with consideration of permafrost dynamics, peatland hydrology, and peatland vegetation. This model was then modified to simulate global net CH₄ emissions for northern peatlands, naturally inundated wetlands and rice agriculture soils (Spahni et al., 2011). To characterize uncertainties and feedbacks between CH₄ flux and climate, Riley et al. (2011) developed a CH₄ biogeochemistry model (CLM4Me) and integrated it into the land component of the Community Earth System Model (CESM), and further analyses were conducted by Meng et al. (2012), but specific plant functional types have not been incorporated in their wetlands. In contrast, Zhu et al. (2014) developed a processed CH₄ biogeochemistry model based on the Integrated Biosphere Simulator (IBIS) (TRIPLEX-GHG), considering plant functional types, but did not consider the emission differences between various wetland types across the landscape. The Global Carbon Project (GCP) and the Wetland and Wetland CH₄ Inter-comparison of Models Project (WETCHIMP) estimated the global methane emission from natural wetlands, ranging from 102 to 284 Tg CH₄ year⁻¹ during 2000–2017 (Kirschke et al., 2013; Melton et al., 2013; Saunois et al., 2016; Saunois et al., 2019).

The above review of the past study suggests that, although significant efforts have been made on development of bottom-up process models, current quantifications of methane emission from natural sources still have large uncertainties. Zhuang et al. (2004) have considered the important freeze-thaw processes and integrated methanogenesis modules into the Terrestrial Ecosystem Model (TEM) to estimate net CH₄ emissions from northern high latitudes. Zhuang et al. (2013) further revised the model and extrapolate it to the global scale to quantify soil methane consumption. The hydrology and soil thermal model (HM and STM) in TEM were revised and evaluated in Liu et al. (2018). In summary, the existing bottom-up estimates still have large uncertainties using various models (Cao et al., 1996; Hodson et al., 2011; Ito & Inatomi, 2012; Kleinen et al., 2012; Melton & Arora, 2016; Ringeval et al., 2010; Spahni et al., 2011; Woodward & Lomas, 2004). Further those estimates have not fully taken advantage of multiple in situ flux data for parameterizing and evaluating their models before conducting global simulations, although a few recent studies have used some site-level observations (Riley et al., 2011; Tian et al., 2010, 2015; Xu et al., 2016; Zhu et al., 2014).

In this study, we made a step forward to use existing flux data at multiple sites to improve our revised methane biogeochemistry model TEM. The revised model was extensively parameterized and verified and

then extrapolated to the global scale. To investigate the uncertainty sources of methane emissions, model simulations were conducted with different sets of parameters and climate forcing and wetland distribution data for the period 2000–2012. Land methane sources and sinks during 1950–2016 were then analyzed.

2. Method

2.1. Overview

We first revised the TEM-MDM model (Zhuang et al., 2003, 2004, 2007, 2013) by considering (1) various types of wetlands based on their plant functional types and climates in boreal, temperate, and tropical regions; (2) the influence of standing water above the surface on methane transport; (3) accumulated vertical methane concentrations in soils; and (4) finer time step in the MDM model (1 hr) and hydrological model (5 min). Second, we used the data of CH₄ flux measurement to calibrate the model with the Shuffled Complex Evolution (SCE-UA) method (Duan et al., 1993) for different wetland types in different climatic regions (Arctic, temperate, and tropical regions). The model was then evaluated using in situ data from different climatic regions. Finally, the model was extrapolated to the globe at a 0.5° by 0.5° resolution. We conducted five sets of model experiments to investigate the impact of parameters, wetland type distribution, climate, atmospheric CH₄, and wetland distribution data on soil CH₄ dynamics: (1) 10 sensitivity simulations by increasing and decreasing: (a) CH₄ surface concentrations by 30%, (b) NPP by 30%, (c) precipitation by 30%, (d) air temperature by 3°C, and (e) inundation area fraction by 30% for each pixel, respectively, while holding other forcing data as they were, during 2000–2012; (2) parameter uncertainty test simulations during 2000–2012; (3) wetland type uncertainty test simulations during 2000–2012; (4) forcing data uncertainty simulations using three sets of climate forcing data and two sets of wetland distribution data during 2000–2012; and (5) historical methane emission and consumption simulations during 1950–2012 to analyze CH₄ responses during El Niño and La Niña events.

2.2. Model Modification

We revised the previous version of TEM-MDM (Zhuang et al., 2003, 2004, 2007, 2013) by considering several more detailed land methane cycling processes. First, standing water effects have not been explicitly modeled previously in TEM-MDM. However, the standing water limits atmospheric oxygen diffusion into soils, reducing oxidation, and affecting methane transport from soils and water column to the atmosphere. In this revision, a new algorithm to account for the effects on methane dynamics was incorporated into TEM-MDM. Specifically, the standing water results in smaller methane diffusivity in water (Tang et al., 2010):

$$D_w = 1.5 \times 10^{-9} \times \left(\frac{T}{298.0} \right) \quad (1)$$

$$D_a = 1.9 \times 10^{-5} \times \left(\frac{T}{298.0} \right)^{1.82} \quad (2)$$

$$D = \frac{1\epsilon D_a + \alpha\theta D_w}{\tau - \epsilon + \alpha\theta} \quad (3)$$

$$\alpha = H \times \frac{T}{12.2} \quad (4)$$

$$H = 1.3 \times 10^{-3} \exp \left[-1700 \left(\frac{1}{T} - \frac{1}{298.0} \right) \right] \quad (5)$$

where the D_w is the diffusivity of methane in water ($\text{m}^2 \text{s}^{-1}$); T is the temperature at each layer (K); D is the combined diffusivity of methane in specific bulk medium ($\text{m}^2 \text{s}^{-1}$); D_a is the diffusivity of methane in air ($\text{m}^2 \text{s}^{-1}$); τ is the tortuosity factor in the soil, taken as 1.5 throughout the study (Arah & Stephen, 1998); ϵ is air-filled porosity ($\text{m}^3 \text{air m}^{-3}$ soil); α is the Bunsen coefficient for methane; θ is the volumetric soil moisture ($\text{m}^3 \text{water m}^{-3}$ soil); H is the Henry's law constant (M atm^{-1}). D is used as diffusivity of methane in the model. We can notice that normally D_a is 1,000 times larger than D_w . Thus, when there is standing water above soil surface, D will be much smaller. Besides, the standing water supplies water to soils and change soil moisture in two situations: (1) when there is standing water above the soil surface, the soil will always be saturated; (2) when there is no standing water, the previous day's standing water will seep into

Table 1

Parameters Related to Methane Production and Oxidation Process for Wetlands in TEM

Name	Meaning	Units	Upper bounds	Lower bounds
M _{GO}	Ecosystem-specific maximum potential CH production rate	μM hr ⁻¹	1	0.1
K _{PCH4}	Methane ecosystem-specific half saturation constant used in Michaelis-Menten kinetics of methane production process	μM	0.2	0.05
P _{Q10}	Ecosystem-specific Q10 coefficient indicating the dependency of CH ₄ production to soil temperature	Unitless	9	1.5
NPP _{MAX}	The maximum monthly NPP expected for a particular vegetation type	gC m ⁻² mon ⁻¹	400	50
L _{MAXB}	Prescribed maximum lower boundary	mm	2,500	900
T _{PR}	The reference temperature for methanogenesis that varies across ecosystems	°C	30	0
O _{MAX}	Ecosystem-specific maximum oxidation coefficient	μM hr ⁻¹	360	0.3
K _{OCH4}	Methane ecosystem-specific half saturation constant used in Michaelis-Menten kinetics of methane oxidation process	μM	66.2	1
O _{Q10}	Ecosystem-specific Q10 coefficient indicating the soil temperature dependency of methanotrophy	Unitless	9	1.5
K _O	Oxygen ecosystem-specific half saturation constant of oxygen used in Michaelis-Menten kinetics of methane oxidation process	μM	200	37
afp	Air-filled porosity of the soil	v/v	0.3	0.1
M _{VMAX}	Maximum volumetric soil moisture for methanotrophy	v/v	1	0.6
M _{VMIN}	Minimum volumetric soil moisture for methanotrophy	v/v	0.3	0
M _{VOPT}	Optimum volumetric soil moisture for methanotrophy	v/v	0.6	0.3
T _{OR}	The reference temperature for methanotrophy that varies across ecosystems	°C	30	0

soils and be treated as extra water supply besides precipitation. In the revised TEM-MDM, the simulated transient standing water is used to account for these effects.

Second, previous TEM-MDM has not considered the effects of accumulated methane in soil columns on methane fluxes. In this study, a new variable was added to record the soil methane concentration accumulation at each time step within each 1-cm soil layer. The effect of adding this variable on soil methane oxidation and transport was incorporated in the model:

1. The changes in CH₄ concentrations are governed by the following equation within each layer:

$$\frac{\partial C_M(z, t)}{\partial t} = M_P(z, t) - M_O(z, t) - \frac{\partial F_D(z, t)}{\partial z} - R_P(z, t) - R_E(z, t) \quad (6)$$

The $C_M(z, t)$ now is the accumulated methane concentration (μM) at z depth of soil (cm) and time t (hr). $\frac{\partial C_M(z, t)}{\partial t}$ is governed by equation 6, where $M_P(z, t)$, $M_O(z, t)$, $R_P(z, t)$, and $R_E(z, t)$ are methane production, oxidation, plant-mediated transport, and ebullition rates, respectively. $\frac{\partial F_D(z, t)}{\partial z}$ represents the flux divergence due to diffusion (μM hr⁻¹).

Soil oxidation was calculated:

$$M_O(z, t) = O_{MAX} f(C_M(z, t)) f(T_{SOIL}(z, t)) f(E_{SM}(z, t)) f(R_{OX}(z, t)) f(N_{dp}(z, t)) f(D_{ms}(z, t)) \quad (7)$$

The Michaelis-Menten kinetics method (Bender & Conrad, 1992) was used to simulate the effect:

$$f(C_M(z, t)) = \frac{C_M(z, t)}{K_{OCH_4} + C_M(z, t)} \quad (8)$$

This equation is similar to equation B1 in Zhuang et al. (2004). The K_{OCH_4} is the methane ecosystem-specific half saturation constant (μM, Table 1). $f(C_M(z, t))$ is used as a multiplier for methane oxidation rate.

Table 2

Calibration (nos. 1–15) and Validation Sites (nos. 16–29) List

No.	Site name	Location (degree)	Type	Climate	Time	Reference
1	SSA-fen	104.62 W, 53.8 N	Peatland, fen	Boreal	Daily 1994–1995	Sellers et al. (1997)
2	NSA-fen	98.42 W, 55.92 N	Peatland, fen	Boreal	Daily 1994/1996	Sellers et al. (1997)
3	Plotnikovo bog	82.85 E, 56.85 N	Nonforested bog	Boreal	Biweekly, June–August in 1997–1998	Glagolev et al. (2011)
4	Plotnikovo mire	82.85 E, 56.85 N	Mire, near river	Boreal	Biweekly, June–August in 2006	Glagolev et al. (2011)
5	Muhrino	68.70 E, 60.89 N	Nonforested bog	Boreal	Biweekly, June–August in 2009–2010	Glagolev et al. (2011)
6	Sallie's fen	71.06 W, 43.21 N	Peatland fen	Temperate	Weekly, 1994–2001	Zhuang and Crill (2008)
7	Buck hollow bog	84.02 W, 42.45 N	Non forested wetland	Temperate	Monthly, 1991–1993	Shannon and White (1994)
8	Minnesota peatland	93.47 W, 47.53 N	Peatland bog	Temperate	Weekly, 1991–1992	Clement et al. (1995), Shurpali et al. (1993), and Shurpali and Verma (1998)
9	Mer Bleue bog	75.48 W, 45.41 N	Nonforested peatland bog	Temperate	Weekly, 2004–2007	Moore et al. (2011)
10	Minnesota peatland	93.47 W, 47.53 N	Peatland bog	Temperate	Monthly, 1988–1990	Dise (1993)
11	Cuini	64.10 W, 0.48–1.14°S	Interfluvial wetlands	Tropical	Monthly 200, 502–200,601	Belger et al. (2011)
12	Itu	63.56 W, 0.29°S	Interfluvial wetlands	Tropical	Monthly 200, 502–200,601	Belger et al. (2011)
13	Earth	83.57 W, 10.22 N	Secondary forest	Tropical	6 visit 2006–2009	Nahlik and Mitsch (2011)
14	La Selva	84.01 W, 10.42 N	Flooded forest	Tropical	6 visit 2006–2009	Nahlik and Mitsch (2011)
15	Palo Verde	85.33 W, 10.34 N	Coastal plains	Tropical	6 visit 2006–2009	Nahlik and Mitsch (2011)
16	Stordalen	19.05°E, 68.33 N	Subarctic micro	Boreal	Monthly, 1974/1994/1995	Svensson et al. (1999)
17	Stordalen	19.05°E, 68.33 N	Subarctic micro	Boreal	Daily, 2006–2007	Jackowicz-Korczyński et al. (2010)
18	Degerö Stormyr	19.55°E, 64.18 N	Boreal mire, fen	Boreal	Daily, 1995–1997	Granberg et al. (2001)
19	Salmisue mire	30.93°E, 62.78 N	Boreal fen	Boreal	Daily, 1997	Saarnio et al. (1997)
20	Ruovesi	24.02°E, 61.83 N	Boreal fen	Boreal	Daily, 2006	Rinne et al. (2007)
21	Quebec	78.77 W, 53.9 N	Peatland	Boreal	Daily, 2003	Pelletier et al. (2007)
22	Quebec	77.72 W, 53.63 N	Peatland	Boreal	Daily, 2003	Pelletier et al. (2007)
23	Quebec	76.13 W, 53.57 N	Peatland	Boreal	Daily, 2003	Pelletier et al. (2007)
24	Sanjiang plain	133.52°E, 47.58 N	Marshland/natural freshwater wetland	Temperate	Annually, 2002–2005	Huang et al. (2010) and Song et al. (2009)
25	Sanjiang plain	133.52°E, 47.58 N	Marshland/freshwater marsh	Temperate	Monthly, 1995–1996, 2001–2003	Wang et al. (2002), Cui (1997), Ding et al. (2004), Yang et al. (2006), and Hao et al. (2004)
26	Loch Vale	105.65 W, 40.28 N	Subalpine wetland	Temperate	Daily, 1996–1998	Wickland et al. (2001)
27	Ryans 1 Billagong	146.97°E, 36.12 N	Freshwater wetland	Temperate	Monthly, Apr 1993–May 1994	Boon and Mitchell (1995)
28	Florida	81.00 W, 25.00 N	Everglade	Tropical	Averaged range using few visits during 1980–1987	Bartlett et al. (1989), Burke et al. (1988), and Harriss et al. (1988)
29	Amazon	Amazon basin	Flooded plain	Tropical	Averaged range using few visits during 1979–1987	Melack et al. (2004), Devol et al. (1988), Bartlett et al. (1988), and Bartlett et al. (1990)

The plant-aided transport basic function is C4 in Zhuang et al. (2004):

$$R_P(z, t) = K_P \cdot \overline{TR}_{VEG} \cdot \overline{f}_{ROOT}(z) \cdot \overline{f}_{GROW}(T_{soil}(z, t)) \cdot \overline{C}_M(z, t) \quad (9)$$

The $C_M(z, t)$ is directly used as a multiplier for plant-aided transport rate calculation. The ebullition transport is simulated in the model using equation C8a in Zhuang et al. (2004):

$$R_E(z, t) = K_e f(C_M(z, t)) \quad (10)$$

The ebullition happens when the $C_M(z, t)$ exceeds a threshold of 500 μM (Walter & Heimann, 2000). The $f(C_M(z, t))$ is equal to the difference between $C_M(z, t)$ and the threshold.

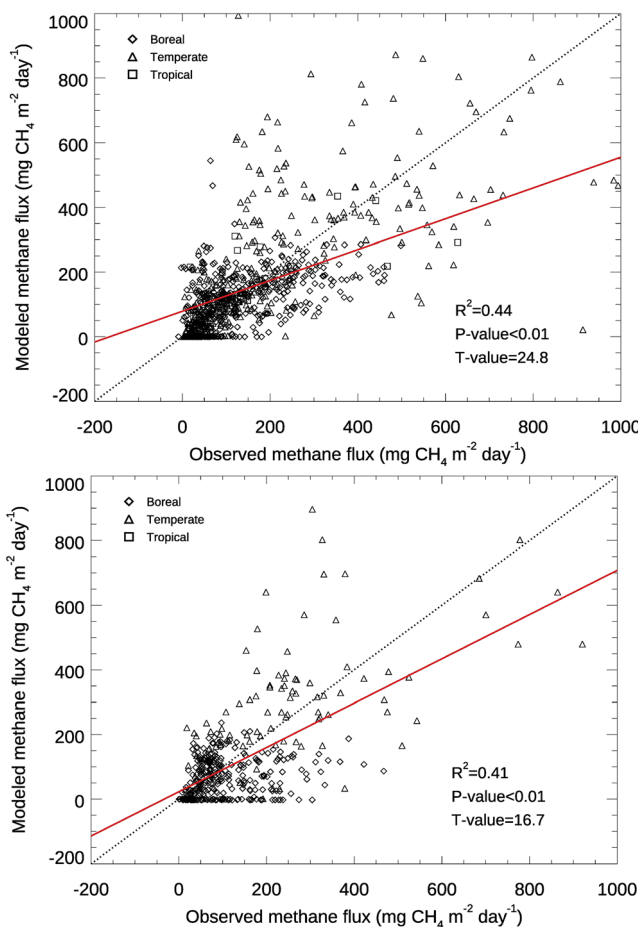


Figure 1. Comparison between observed and simulated methane fluxes at calibration sites (upper panel) and evaluation sites (lower panel). Diamond symbol represents the boreal data. Triangle symbol represents the temperate data. Square symbols represent the tropical data. Dot line represents that the observed data equal the simulated data. Red solid line represents the linear regression line between all observed and simulated data.

set of Global Summary of the Day (GSOD) (<http://www7.ncdc.noaa.gov/CDO/cdoselect.cmd?datasetabbv=GSOD&countryabbv=&georegionabbv=>) to drive the model, and the station IDs are 020200, 020200, 022740, 029290, 029450, 716,278, 718,270, 718,113, 724,675, and 948,990, respectively. For sites no. 18, we used the station 022860 together with 022740 to fill the missing data of precipitation. If the data from GSOD missed a few days of observation, we would fill the missing points by linear interpolation. For longer data gaps (longer than 15 days), we filled the data with CRU data. For other sites, we used CRU data to drive the model. Since the GSOD data did not provide cloud fraction or solar radiation data, we used the CRU cloud fraction data for all sites. Vegetation type, wetland type, soil texture, and elevation information have been set based on site observations.

2.4. Data Organization

To get the spatially and temporally explicit estimates of CH₄ consumption and emission at the global scale, we used the data of land cover, soils, climate, and leaf area index (LAI) from various sources at a spatial resolution of 0.5° latitude × 0.5° longitude to drive TEM-MDM. The land cover data include the potential vegetation distribution (Melillo et al., 1993) and soil texture (Zhuang et al., 2003), which were used to assign vegetation- and texture-specific parameters to each grid cell.

In addition, instead of the daily time step applied in previous model, we used 5-min time step for TEM hydrology module and 1-hr time step for methane dynamics because water and gases can change rapidly at fine time steps (Bonan, 1996). Finer time steps will reduce partial differential equation (PDE) solution errors. Previous model was only developed for boreal regions (Zhuang et al., 2004). In order to extrapolate the model to global scale, we used the climate types and five wetland classification types from Matthews and Fung (1987), including forested bog, nonforested bog, forested swamp, nonforested swamp, and alluvial formation, to represent wetland types across the landscape. Climate types were determined by site description (site-level simulation) or its latitude (regional simulation, tropical <30°, 30° <temperate <60°, and boreal >60° for both hemispheres). With the three types of climate and five types of wetlands, we totally have 15 types of wetlands for model simulations.

2.3. Model Parameterization and Extrapolation

Wetland methane production and oxidation processes involve 15 key parameters in TEM-MDM (Table 1). TEM-MDM was calibrated by running it for observational periods driven with the corresponding meteorological data at each site (Table 2 and Figure 1 upper panel) and using the Shuffled Complex Evolution Approach in R language (SCE-UA-R) (Duan et al., 1993) to minimize the difference between the simulated and observed net CH₄ fluxes. Each site was run 50 times using the SCE-UA-R with 10,000 maximum loops, and all of them reached a stable state before the end of the loops. In addition to using in situ meteorological and soil data, we also used the ERA-interim reanalysis data from the European Centre for Medium-Range Weather Forecasts (ECMWF), and reanalysis climatic data from Climatic Research Unit (CRUTS4.01, Harris et al., 2014, CRU for short) to fill any missing environmental data. Parameter values for various wetland types were summarized in supporting information Table S1. Revised model performance will be discussed in section 4.1, and time series comparisons between the revised version model, previous model, and observations are presented in Figures S1 and S2.

The parameterized model was then evaluated at 14 sites (nos. 16–29 in Table 2), located in different climatic regions. For sites nos. 16–23, 26, and 27, we used nearest stations to the evaluation sites in the global data

Table 3
Model Evaluations With Observations

	Site 16	Site 17	Site 18	Site 19	Site 20	Site 21	Site 22	Site 23	Site 24	Site 25	Site 26	Site 27
Observation points	9	42	24	80	127	7	7	7	6	31	53	14
Observed mean value	77.81	117.19	72.27	190.30	53.51	79.94	28.01	28.11	117.84	383.15	172.67	186.48
RMSE	64.90	104.31	46.81	153.40	42.68	91.92	68.99	48.96	83.96	270.59	101.78	83.33
R^2	0.30	0.00	0.24	0.07	0.55	0.49	0.19	0.72	0.18	0.18	0.56	0.66
P value	0.12	0.95	0.02	0.01	0.00	0.08	0.33	0.02	0.40	0.02	0.00	0.00
T test	1.75	0.07	2.61	2.49	12.29	2.17	1.08	3.62	0.95	2.53	8.20	4.73

Note. Observation points are acceptable observed flux data at each site. RMSE is root mean square error between simulation and observation ($\text{mg CH}_4 \text{ m}^{-2} \text{ day}^{-1}$). R^2 is the coefficient of determination. P value is the probability value based on a two-sided t test. T value is the t statistic value. Regional results from sites 28 and 29 are discussed in section 3.1.

In order to map the global methane fluxes from natural wetland and investigate the uncertainties from different sources, we used climate forcing data including the monthly CRU data during 1950–2012, the daily ERA Interim data from European Centre for Medium-Range Weather Forecasts (ECMWF; Dee et al., 2011), during 2000–2012, and the daily reanalysis data from National Centers for Environmental Prediction (NCEP; Kalnay et al., 1996) during 2000–2012 (Figure S3). The resolutions of CRU and ECMWF data are 0.5° latitude $\times 0.5^\circ$ longitude. The NCEP data with an original spatial resolution of 2.5° latitude $\times 2.5^\circ$ longitude were re-gridded to 0.5° latitude $\times 0.5^\circ$ longitude resolution. We also used wetland distribution data including static wetland map from Matthews and Fung (1987) (M&F), and the transient wetland inundation area fraction data derived from previous study of merging Surface WAtter Microwave Product Series (SWAMPS; Schroeder et al., 2015) with the static inventory of wetland area from the Global Lakes and Wetlands Database (GLWD; Lehner & Döll, 2004) by Poulter et al. (2017) (SWAMPS-GLWD) during 2000–2012 (Figure S4). The spatial resolutions of these data sets are 0.5° latitude $\times 0.5^\circ$ longitude. Observed CO₂ concentrations from in situ air measurements taken at Mauna Loa Observatory by Earth System Research Lab of National Oceanic and Atmospheric Administration (NOAA/ESRL, <https://www.esrl.noaa.gov/gmd/ccgg/trends/data.html>) were used for the period covering 1958–2012. Observed atmospheric CH₄ concentration data from NOAA/ESRL (www.esrl.noaa.gov/gmd/ccgg/trends_ch4/) cover 1984–2012. CO₂ data before 1984 were from summary of U.S. Environment Protection Agency (EPA, <https://www.epa.gov/climate-indicators/climate-change-indicators-atmospheric-concentrations-green-house-gases>). El Niño and La Niña event data were derived from Zhu et al. (2017).

2.5. Model Experimental Design

To investigate the uncertainty from different sources, we conducted five experiments: (1) the sensitivity and correlations during 2000–2012 using CRU and SWAMPS_GLWD data. Ten sensitivity simulations were driven with varying different forcing variables while keeping others as they were, by increasing or decreasing: (a) CH₄ surface concentrations by 30%, (b) NPP by 30%, (c) precipitation by 30%, (d) air temperature by 3°C , and (e) inundation area fraction by 30% for each pixel, respectively, during 2000–2012. The magnitudes of changes in the input data were chosen to ensure they do not exceed the values identified in the field or based on previous model studies (Liu et al., 2018; Zhuang et al., 2004; Zhuang et al., 2013). Modifications were applied to the forcing data by multiplying a factor (e.g., 1.3 to NPP) to every value used in model simulations. Correlations were calculated from sensitivity baseline simulation (experiment E1); (2) the uncertainty of parameters during 2000–2012 using CRU and SWAMPS-GLWD data. We conducted 100 simulations with parameters randomly chosen in optimized ranges and compared the results with the baseline simulation which uses the mean value of each parameter (experiment E2); (3) the uncertainty of wetland type distribution during 2000–2012 using CRU and SWAMPS-GLWD data. M&F wetland data could only identify the wetland type for half of the pixels. Other pixels could have a period with inundated area as SWAMPS-GLWD indicated and were first grouped by their climate and vegetation types. Each group would then randomly choose possible wetland types. In this way, totally 770 simulations were conducted with different wetland type distributions (experiment E3); (4) the uncertainty from forcing data using CRU, ECMWF, NCEP, M&F wetland data, and SWAMPS-GLWD inundation data during 2000–2012. Six forcing data uncertainty test simulations were driven with different forcing data sets while keeping others as they were (a) using CRU climate data with static M&F wetland data and transient SWAMPS-GLWD

Table 4
Model Sensitivity Test During 2000–2012 Using Monthly CRU Data and Transient Wetland Fraction Data

Flux type	Region	Value	Baseline ($\text{CH}_4 \text{ year}^{-1}$)	$\text{CH}_4 + 30\%$	$\text{CH}_4 - 30\%$	NPP	NPP +30%	Precipitation	Precipitation -30%	Air T	Air T +3°C	Air T -3°C	Inundation fraction	Inundation fraction +30%	Inundation fraction -30%
Consumption	Global	Value	-35.33	-40.83	-29.61	-35.92	-34.75	-36.74	-33.62	-54.11	-25.62	-35.02	-35.73		
		Change %	0.00	15.57	-16.19	1.67	-1.64	3.99	-4.84	53.16	-27.48	-0.88	1.13		
90–45°S	Value	-0.14	-0.18	-0.1	-0.14	-0.14	-0.15	-0.15	-0.14	-0.15	-0.13	-0.14	-0.14		
	Change %	0.00	28.57	-28.57	0.00	0.00	7.14	0.00	7.14	7.14	-7.14	0.00	0.00	0.00	
45°S to 0	Value	-5.95	-7.22	-4.65	-6	-5.9	-6.42	-5.5	-7.76	-5.09	-5.93	-5.93	-5.99		
	Change %	0.00	21.34	-21.85	0.84	-0.84	7.90	-7.56	30.42	-14.45	-0.34	-0.34	0.67		
0–45 N	Value	-22.62	-25.34	-19.7	-23.04	-22.2	-23.41	-21.61	-27.37	-15.36	-22.39	-22.39	-22.86		
	Change %	0.00	12.02	-12.91	1.86	-1.86	3.49	-4.47	65.21	-32.10	-1.02	-1.02	1.06		
45–90 N	Value	-6.62	-8.09	-5.15	-6.74	-6.51	-6.76	-6.37	-8.83	-5.05	-6.55	-6.55	-6.73		
	Change %	0.00	22.21	-22.21	1.81	-1.66	2.11	-3.78	33.38	-23.72	-1.06	-1.06	1.66		
Emission	Global	Value	211.93	210.5	213.36	222.27	201.59	215.15	206.89	309.54	146.03	266.51	148.33		
	Change %	0.00	-0.67	0.67	4.88	-4.88	1.52	-2.38	46.06	-31.10	25.75	25.75	-30.01		
90–45°S	Value	0.57	0.57	0.58	0.6	0.54	0.58	0.57	0.92	0.38	0.74	0.74	0.4		
	Change %	0.00	0.00	1.75	5.26	-5.26	1.75	0.00	61.40	-33.33	29.82	29.82	-29.82		
45°S to 0	Value	44.71	44.33	45.09	47.29	42.13	46.05	41.3	60.38	33.1	54.22	31.29			
	Change %	0.00	-0.85	0.85	5.77	-5.77	3.00	-7.63	35.05	-25.97	21.27	21.27	-30.02		
0–45 N	Value	124.72	124.11	125.32	129.24	120.19	126.11	123.32	184.34	85.32	157.51	157.51	87.29		
	Change %	0.00	-0.49	0.48	3.62	-3.63	1.11	-1.12	47.80	-31.59	26.29	26.29	-30.01		
45–90 N	Value	41.93	41.5	42.37	45.14	38.73	42.41	41.69	63.91	27.23	54.03	54.03	29.35		
	Change %	0.00	-1.03	1.05	7.66	-7.63	1.14	-0.57	52.42	-35.06	28.86	28.86	-30.00		

Table 5

Correlations Between Simulated Methane Fluxes and Environmental Factors During 2000–2012 Using Monthly CRU Data and Transient Wetland Fraction Data

Variable name	CH ₄ dynamics	Month correlation					Year correlation				
		South—45°S	45°S to 0	0–45 N	45 N—north	Global	South—45°S	45°S to 0	0–45 N	45 N—north	Global
NPP	Consumption	−0.86	−0.87	−0.86	−0.96	−0.95	0.52	0.04	0.23	0.17	0.38
	Emission	0.70	0.83	0.89	0.99	0.99	−0.04	0.23	0.30	−0.32	0.10
PREC	Consumption	0.15	−0.91	−0.94	−0.90	−0.84	−0.56	0.31	−0.20	−0.20	−0.04
	Emission	−0.28	0.90	0.94	0.87	0.78	−0.05	−0.35	0.18	−0.05	−0.24
TAIR	Consumption	−0.83	−0.85	−0.88	−0.96	−0.89	0.08	−0.54	0.27	−0.77	−0.27
	Emission	0.83	0.91	0.93	0.88	0.90	0.71	0.58	0.38	0.53	0.73
IN_AREA	Consumption	0.68	−0.41	−0.64	−0.93	−0.89	−0.07	−0.71	−0.42	−0.42	−0.68
	Emission	−0.49	0.48	0.76	0.87	0.92	−0.15	0.68	−0.21	0.60	0.41
TSOIL	Consumption	−0.83	−0.85	−0.89	−0.99	−0.92	0.07	−0.54	0.30	−0.71	−0.10
	Emission	0.83	0.91	0.94	0.92	0.92	0.71	0.59	0.42	0.70	0.74
VSOIL	Consumption	0.52	−0.77	−0.52	−0.88	−0.77	−0.45	−0.67	−0.72	−0.20	−0.80
	Emission	−0.48	0.76	0.48	0.79	0.77	−0.25	0.51	−0.14	−0.09	−0.10

Note. Factors include net primary production (NPP), precipitation (PREP), air temperature (TAIR), wetland inundation area fraction (IN-AREA), soil temperature (SOILT), and volumetric soil moisture (VSOIL).

inundation data, (b) using ECMWF climate data with static M&F wetland data and transient SWAMPS-GLWD inundation data, and (c) using NCEP climate data with static M&F wetland data and transient SWAMPS-GLWD inundation data (experiment E4); and (5) historical methane emission and consumption simulation using CRU data during 1950–2012 and compare to El Niño and La Niña events. The inundation area fraction data for the period 2000–2012 are from SWAMPS-GLWD data. We used the inundation data of year 2000 to represent the inundation distribution and area for each year during 1950–1999 (experiment E5).

3. Results

3.1. Site Calibration and Evaluation

We use $p < 0.05$, $t > 2.0$, and relatively large R^2 to determine if the model simulations are well correlated with the observation at calibration sites. Our overall calibration and evaluation results are significant. The R^2 is 0.44 with $p < 0.01$ and $T = 24.8$ for overall calibration results. R^2 is 0.41 with $p < 0.01$ and $t = 16.7$ for overall evaluation results. For most sites, the model captures the magnitude and the variation of the observation in model evaluations (Table 3). Significant correlations are found for most sites except three sites from the boreal region (site 16, 17, and 22) and one site from the temperate region (site 24, Table 3). The poor performance for those sites is discussed in section 4.1. The simulated and observed mean values are comparable with root mean square errors (RMSE) less than $270 \text{ mg CH}_4 \text{ m}^{-2} \text{ day}^{-1}$. For site 28 and 29, simulations indicate the average emissions are $25 \text{ mg CH}_4 \text{ m}^{-2} \text{ day}^{-1}$ with variation of $14 \text{ mg CH}_4 \text{ m}^{-2} \text{ day}^{-1}$, while observations range from 4 to $217 \text{ mg CH}_4 \text{ m}^{-2} \text{ day}^{-1}$.

3.2. Sensitivity Analysis

Modeled methane emissions are sensitive to NPP, air temperature, and inundation area fraction globally and also sensitive to precipitation in 45°S to 0 latitude regions. Simulated methane consumption is sensitive to atmospheric methane concentration, precipitation, and air temperature (Table 4). Simulated methane emissions are highly correlated with NPP, air temperature, inundation area fraction, and soil temperature globally, while methane consumption is highly correlated with NPP, precipitation, air temperature, inundation area fraction, and soil temperature globally. Annual correlations showed that the interannual variability of methane emissions are correlated with air temperature and soil temperature, while the interannual variability of methane consumption is correlated with inundation area fraction and soil moisture (Table 5).

3.3. Global Emission Uncertainty Due to Uncertain Parameters

Global gross methane emission uncertainty increases during summer and decreases in winter, with a large uncertainty range surrounding the baseline simulation (Figure 2a). Globally, annual methane emission mean values (red dots) are close to the baseline with standard deviation (STD) of $62 \text{ Tg CH}_4 \text{ year}^{-1}$

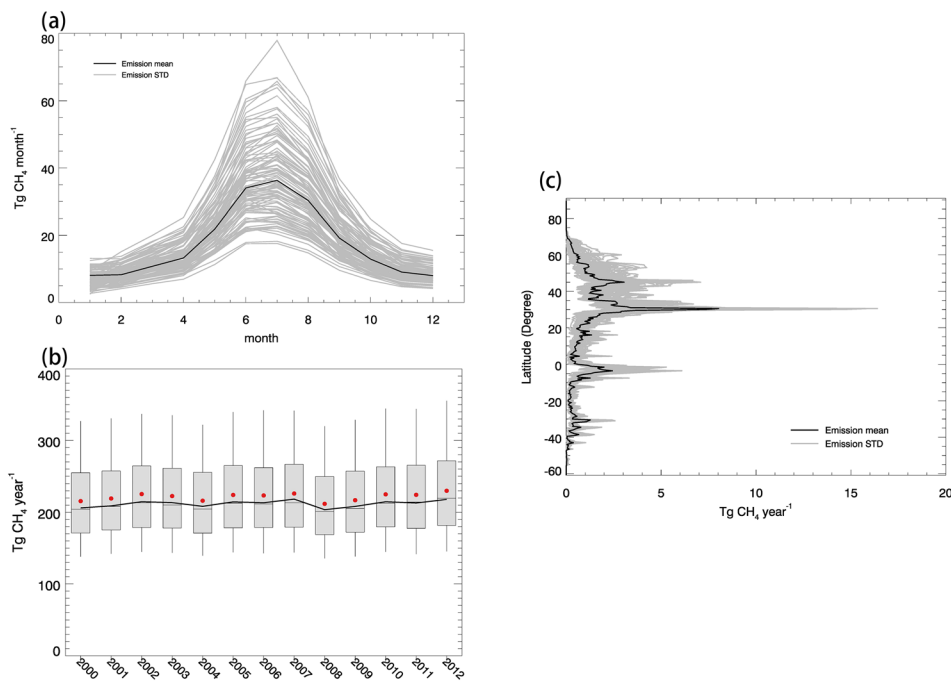


Figure 2. Parameter uncertainty analysis during 2000–2012: (a) global monthly methane flux uncertainties, the black line represents the baseline results, and the gray lines represent the 100 simulation results using parameters which were randomly chosen in optimized ranges; (b) global annual methane flux uncertainties, the black line represents the baseline. For each box, line top, box top, horizontal line inside box, box bottom, and line bottom represent maximum, third quartile, median, first quartile, and minimum of 100 simulations, respectively; and (c) the latitude distribution of global annual mean methane emissions, the black line represents the baseline results, and the gray lines represent the 100 parameter uncertainty simulations.

(Figure 2b and Table 6). Temperate forest bog (type 6), tropical forested swamps (type 13), and boreal forested bog (type 1) contribute most of the uncertainty due to their uncertain parameters, with annual mean STDs of 23, 22, and 15 $Tg\text{CH}_4\text{ year}^{-1}$, respectively (Table 6). The temperate region ($0\text{--}45^\circ\text{N}$) in Northern Hemisphere contributes most to the parameter uncertainties while boreal region ($45\text{--}90^\circ\text{N}$) in the Northern Hemisphere contributes second most, with annual mean STDs of 40 and 19 $Tg\text{CH}_4\text{ year}^{-1}$, respectively (Figure 2c and Table 7).

Table 6
Parameter Uncertainties in Different Wetland Types

Type numbers	Climate	Subtype	Pixels	Annual mean emission ($Tg\text{CH}_4\text{ year}^{-1}$)	Annual mean STD ($Tg\text{CH}_4\text{ year}^{-1}$)
1	Boreal	Forested bog	11,475	13.95	14.96
2	Boreal	Nonforested bog	10,050	3.14	1.68
3	Boreal	Forested swamp	52	0.01	0.01
4	Boreal	Nonforested swamp	164	0.25	0.14
5	Boreal	Alluvial formations	1	0.00	0.00
6	Temperate	Forested bog	6,754	48.12	23.42
7	Temperate	Nonforested bog	4,340	18.72	7.34
8	Temperate	Forested swamp	1,101	23.54	11.87
9	Temperate	Nonforested swamp	741	4.56	2.19
10	Temperate	Alluvial formations	72	1.07	0.42
11	Tropical	Forested bog	55	1.58	1.02
12	Tropical	Nonforested bog	8,538	19.72	6.70
13	Tropical	Forested swamp	12,791	37.13	21.78
14	Tropical	Nonforested swamp	5,431	7.11	2.32
15	Tropical	Alluvial formations	206	7.73	4.68
Total	—	—	61,771	211.93	62.04

Table 7

Simulated Methane Emission ($\text{Tg CH}_4 \text{ Region}^{-1} \text{ year}^{-1}$) Uncertainties Due to Uncertain Parameters and Wetland Type Distribution Expressed with Standard Deviations (STD) in Different Regions

	90–45°S	45°S to 0	0–45 N	45–90 N	Global
Emission baseline	0.58	44.84	124.28	41.7	211.93
Emission parameter uncertainty STD	0.34	15.11	40.44	19.3	61.82
Emission wetland type uncertainty STD	0.11	7.24	25.77	3.61	31.93

3.4. Global Emission Uncertainty Due to Uncertain Wetland Type Distribution

Global gross methane emission uncertainty due to uncertain wetland type distribution increases during summer and decreases in winter, with a large uncertainty range surrounding the baseline simulation (Figure 3a). Globally, methane emissions are lower than the baseline with STD of $32 \text{ Tg CH}_4 \text{ year}^{-1}$ (Figure 3b and Table 7). The temperate region ($0\text{--}45^\circ\text{N}$) in the Northern Hemisphere contributes most to the wetland type uncertainty (Figure 3c and Table 7).

3.5. Uncertainty Due to Uncertain Forcing Data

Driven with CRU data, the global wetland methane emissions are 186 and $212 \text{ Tg CH}_4 \text{ year}^{-1}$ by using M&F static wetland distribution data and SWAMPS-GLWD dynamical inundation data, respectively, during 2000–2012. The respective emissions using static and dynamic inundation data are 195 and $210 \text{ Tg CH}_4 \text{ year}^{-1}$ driven by NCEP data, and 195 and $212 \text{ Tg CH}_4 \text{ year}^{-1}$ driven by ECMWF data (Table 8 and Figure 4). These experiments result in the global wetland emissions ranging from 186 to $212 \text{ Tg CH}_4 \text{ year}^{-1}$ for the study period. The global soil consumption ranges from -34 to $-46 \text{ Tg CH}_4 \text{ year}^{-1}$, resulting in global net land methane budget ranging from 149 to $176 \text{ Tg CH}_4 \text{ year}^{-1}$ during 2000–2012 (Table 8). Among these simulations the seasonal emissions and consumption are similar, while emissions from using transient inundation area fraction data are always higher during summer and lower during winter comparing with the simulations using static wetland data (Figure 4, upper panel). The peak value of seasonal emissions has shifted a little from July to June when using transient wetland data (Figure 4, upper panel). Using different wetland distribution data result in large differences in global emissions (Figure 4, lower panel). Methane emissions from simulations using CRU and static wetland map are lowest in all simulations (Figure 4, lower

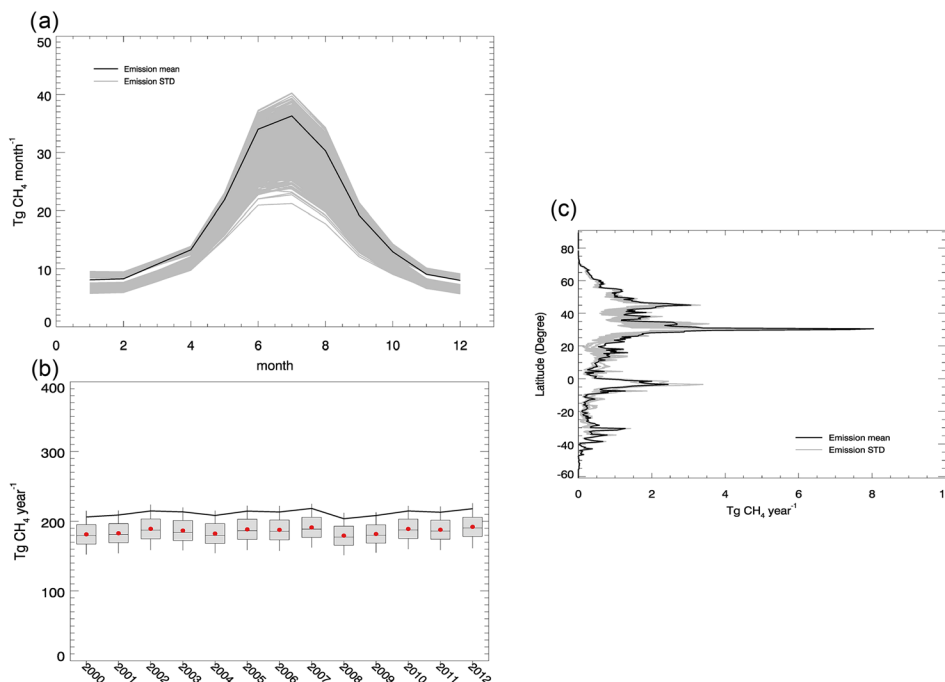


Figure 3. Wetland type uncertainty analysis during 2000–2012: (a) global monthly methane flux uncertainties, the black line represents the baseline results, and the gray lines represent the 770 simulation results using different wetland distributions; (b) global annual methane flux uncertainties, the black line represents the baseline. For each box, line top, box top, horizontal line inside box, box bottom, and line bottom represent maximum, third quartile, median, first quartile, and minimum of 770 simulation results, respectively; and (c) the latitude distribution of global annual mean methane emission, the black line represents the baseline results, and the gray lines represent the results of the 770 wetland type uncertainty simulations.

Table 8

Modeled Methane Fluxes ($\text{Tg CH}_4 \text{ year}^{-1}$) Uncertainties Due to Different Forcing Data

Flux type	Region	CRU Static	CRU Transient	ECMWF Static	ECMWF Transient	NCEP Static	NCEP Transient
Consumption	90–45°S	-0.19	-0.14	-0.26	-0.16	-0.29	-0.19
Consumption	45°S to 0	-7.49	-5.99	-9.86	-6.93	-10.38	-7.1
Consumption	0–45 N	-16.76	-22.72	-20.9	-27.27	-23.22	-27.51
Consumption	45–90 N	-9.44	-6.64	-11.69	-7.54	-12.14	-7.64
Emission	90–45°S	0.22	0.57	0.2	0.55	0.14	0.55
Emission	45°S to 0	53.76	44.67	51.39	40.05	53.73	42.59
Emission	0–45 N	52.24	124.75	55.31	122	51.75	121.22
Emission	45–90 N	79.57	41.96	87.89	47.4	89.18	47.91
Consumption	Global	-33.89	-35.48	-42.71	-41.89	-46.04	-42.43
Emission	Global	185.78	211.93	194.78	210.01	194.81	212.27

panel). Regional distributions for forcing data test can be found in Figures S5 and S6. Methane emissions are similar when using different climate forcing data but have large differences when using different inundation data (Figures S5a, S5c, and S5e). Methane emission flux increases in regions like middle of Northern America and Eastern Asia and decreases in regions like northern high latitudes (Figures S5b, S5d, and S5f). Methane consumptions increase in Europe, Eastern United States, and Eastern Asia when using ECMWF and NCEP climate forcing and comparing with baseline with CRU climate forcing (Figures S6a, S6c, and S6e). When using transient wetland inundation data, the methane consumption fluxes increases in temperate region of the Northern hemisphere and Eastern Australia and decreases in boreal region of the Northern Hemisphere and tropical regions (Figures S6b, S6d, and S6f).

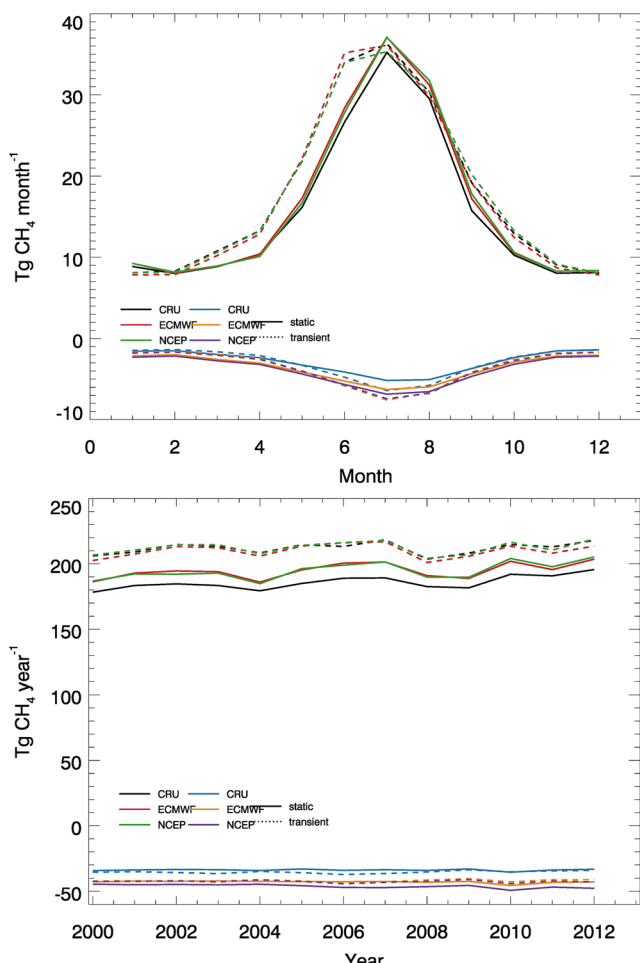


Figure 4. Forcing data uncertainty test results during 2000–2012: Upper panel represents global monthly methane flux uncertainties. Different colors and line styles represent different combinations of forcing data; lower panel represents global annual methane flux uncertainties. Different colors and line styles represent different combinations of forcing data.

3.6. Global Land Methane Budget Estimates During 1950–2012

Model estimates of annual methane emissions are $198 \text{ Tg CH}_4 \text{ year}^{-1}$ and consumption is $-32 \text{ Tg CH}_4 \text{ year}^{-1}$ during 1950–2012 (Table 9). Temperate regions ($0\text{--}45^\circ\text{N}$) contribute most to the global methane emission and consumption (Table 9). Eastern United States, Eastern Asia, and Amazonia regions are emission hotspots, while consumption hotspots are Eastern United States, Middle East, and eastern China (Figures 5a and 5b). For instance, three methane emission peaks show up around 30°N , 45°N , and the equator, while one consumption peak shows around 35°N (Figure 5c). Temporally, both methane emission and the consumption increased during El Niño events and decreased during La Niña events (Figure 6).

4. Discussion

4.1. Site-Level Model Performance

Calibrations and evaluations were conducted for the revised model as described in section 2.3. The calibrated earlier version of TEM-MDM only for northern high latitudes (Zhuang et al., 2004) was used for daily evaluation at boreal sites. Here we evaluated both models for sites in different regions of the globe. While the revised model generally captured the observations with R^2 of 0.44 and 0.41 for calibration and validation, respectively (Figure 1), there were a few discrepancies between simulations and observations. First, most of the model biases can be found at temperate sites (Figure S1). The reason is

Table 9 Modeled Methane Fluxes ($Tg\ CH_4\ year^{-1}$) During 1950–2012 Using CRU Data					
	90–45°S	45°S to 0	0–45 N	45–90 N	Global
Emission value	0.55	41.60	116.65	38.90	197.70
Emission (%)	0.28	21.04	59.00	19.67	100.00
Consumption value	-0.14	-5.16	-20.49	-5.86	-31.65
Consumption (%)	0.44	16.29	64.76	18.51	100.00

that during summer, some temperate sites can emit large amounts of methane ($\sim 1,000\ mg\ CH_4\ m^{-2}\ day^{-1}$; Figure S1) due to suitable soil hydrology condition and high temperature, which were hardly captured by the model. Second, at some sites, observations show positive values, but simulations are near zero (Figure 1). The reason is that our revised model shuts down methane production when soil temperature is below $0^{\circ}C$. However, during winter, some sites can still produce methane based on field observations (Figures S1 and S2).

TEM-MDM might have also estimated a lower temperature than field observations (Liu et al., 2018). The forcing data used in site-level simulations can also induce errors, because some sites do not have sufficient observed forcing data, but using reanalysis data from CRU or ERA Interim from ECMWF. Third, the revised model performed poorly at monthly site 16 and annually site 24, due to coarse simulation time steps and using reanalysis forcing data or averaged forcing data instead of meteorological data. The daily site 17 and site 22 simulations missed emission peaks (Figures S2a and S2f). The reason is that the climate data from the nearest GSOD station have been used for these two sites, but they may not well represent the real environment conditions. Fourth, the earlier TEM-MDM often overestimated methane emissions from wetlands during summer for boreal sites (Figures S2a–S2g). The reasons are several folds: (1) The model does not consider the accumulated substrate methane concentration effects. The oxidation in the unsaturated zone will be underestimated using equation 8; (2) the coarse time step for hydrology model causes too much water infiltrating into soils, overestimating water table depth; and (3) the coarse time step for methane dynamics may also cause a large methane gradient between topsoil layer and the atmosphere, overestimating the diffusion from soils to the atmosphere. At temperate site 26, the earlier version underestimated the fluxes by not including proper climate and wetland type.

4.2. Major Controls to the Global Land Methane Budget

Methane emissions are globally sensitive to changes in NPP, air temperature, and wetland distributions (Table 4). The global annual emissions are more than five times larger than consumption. Of the three major controls, methane emissions are relatively more sensitive to air temperature, varying 46% or -31% when temperature is increased by 3 or decreased by $-3^{\circ}C$ (Table 4). Methane emissions are also sensitive to the

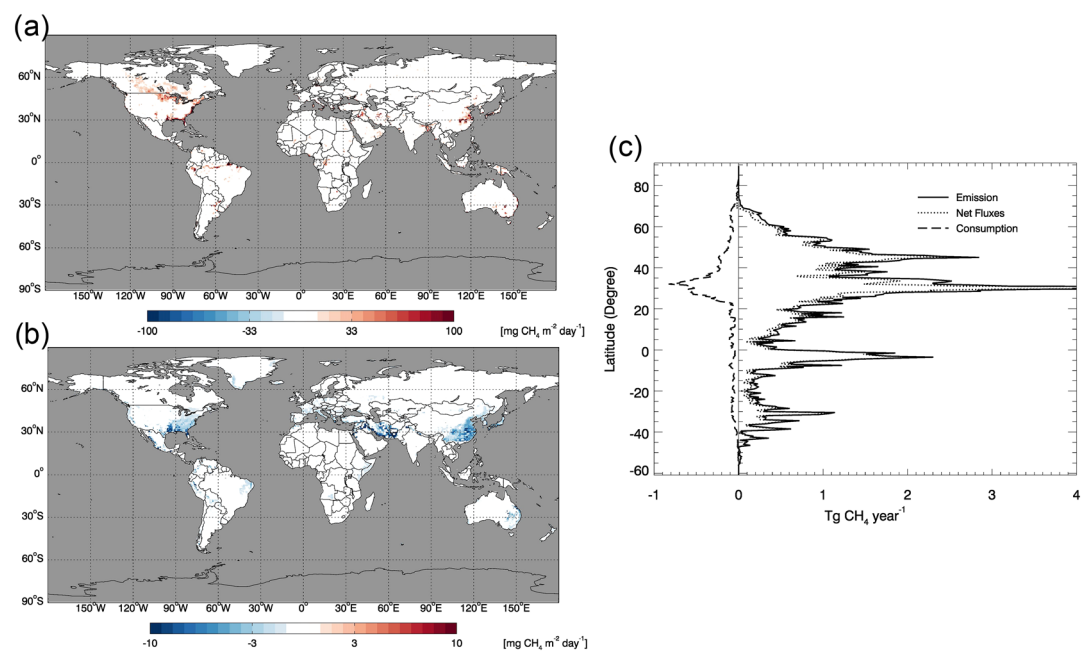


Figure 5. Global simulation during 1950–2012 using CRU data and transient wetland fraction data: (a) global distribution of annual wetland methane emissions; (b) global distribution of annual upland methane consumption; and (c) latitude distribution of methane emission, consumption, and net fluxes.

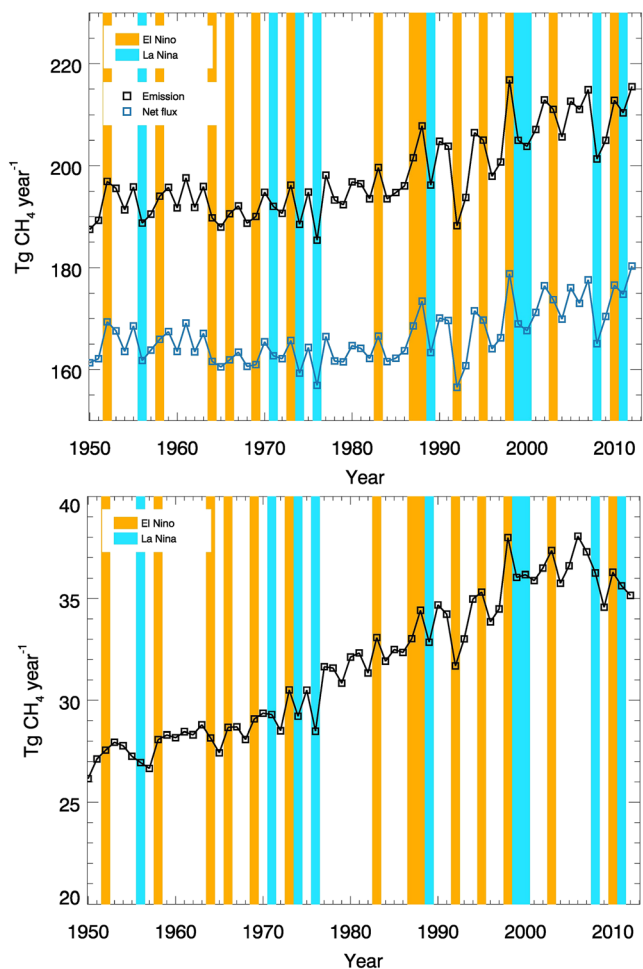


Figure 6. Historical estimates and comparisons: Upper panel represents annual wetland methane emissions (black) and net fluxes (blue) during El Niño (yellow strip) and La Niña (blue) event periods; lower panel represents annual upland methane consumption (black) during El Niño (yellow strip) and La Niña (blue) event periods.

tainty during winter (up to $7 \text{ Tg CH}_4 \text{ mon}^{-1}$ during December, January, and February, Figures 2a and 3a). The reason is that methane emissions are higher during summer in the Northern Hemisphere which has higher wetland inundation area fraction (Figure S4), with large anomalies (75–100% quantile) below base line estimates (Figure 3b). Globally the uncertain parameters result in $62 \text{ Tg CH}_4 \text{ year}^{-1}$ methane emissions while the uncertain wetland type results in $32 \text{ Tg CH}_4 \text{ year}^{-1}$ in our estimates. The temperate forested bog, tropical forested swamp, and boreal forested bog are three main sources of the parameter uncertainties, emitting 23 , 22 , and $15 \text{ Tg CH}_4 \text{ year}^{-1}$, respectively, due to their relatively high rate of methane emissions and a large number of pixels ($12,791$, $6,754$, and $11,475$, respectively, Table 6). There are some types containing a small number of pixels, such as boreal forested swamp (52), boreal alluvial formations (1), temperate alluvia formations (72), and tropical forested bog (55). Northern temperate regions (0 – 45°N) contribute most to the parameter and wetland type uncertainty, emitting 40 and $26 \text{ Tg CH}_4 \text{ year}^{-1}$, respectively, due to the biggest emission rates (higher than $1,000 \text{ mg CH}_4 \text{ m}^{-2} \text{ day}^{-1}$ during summer, Figure S1) over this region and their diverse vegetation types (Table 7).

In order to investigate the forcing data influences on methane emission and production, we used different sources of climate and wetland distribution data (Figures S3 and S4). CRU data have higher global average air temperature and lower precipitation. We used cloud fraction data instead of solar radiation (Figure S3). It shall be noticed that the ECMWF solar radiation data are always lower than NCEP data. We use 12 hr average solar radiation data from ECMWF and use average of daily data from NCEP. The wetland distribution

change in wetland distribution, resulting in 25% or -30% changes when the inundation area increased or decreased by 30% (Table 4). Methane emissions are not sensitive to the precipitation globally, which only change 1.5% and -2.4% when adjusting precipitation by 30% but are sensitive in some specific regions such as 45°S to 0 , which change 3.0% and 7.6% (Table 4). The reason is that only the water table depth or standing water will influence the methane production in soils, and the water table depth is not calculated linearly in our model, which is significantly influenced by temperature (Zhuang et al., 2004, 2013). Besides, the wetland distribution overlaps with the sensitivities of precipitation to some extent. The correlations show that methane emissions are highly correlated with NPP, air temperature, wetland inundation area fraction, and soil temperature ($R > 0.9$, Table 5). This is mainly due to the fact that most of these variables share the same pattern as air temperature, which is high in summer and low in winter. Methane emissions are only correlated well with air temperature and soil temperature ($R > 0.6$, Table 5).

Methane consumption is most sensitive to air temperature (change 53% and -26% , Table 4). This is mainly due to the treatment that Q10 function used in the model as temperature influences methane consumption (Zhuang et al., 2004, 2013). Methane consumption is sensitive to atmospheric methane concentration (changes by 16% and -16% , Table 4). The methane consumption is also sensitive to precipitation globally comparing with the emission sensitivity (changes by 4% and -5% , Table 4) (Zhuang et al., 2004, 2013). The monthly methane consumption is well correlated with NPP, air temperature, soil temperature, and wetland inundation fraction ($|R| \geq 0.9$). In contrast, annual methane consumption is only correlated with wetland inundation area fraction and soil moisture ($|R| > 0.6$, Table 5). Wetland inundation area fraction influences the area of upland in each pixel, affecting methane consumption.

4.3. Model Uncertainty Sources

Methane emissions have a larger uncertainty during summer (up to $45 \text{ Tg CH}_4 \text{ mon}^{-1}$ during June, July, and August) and lower uncertainty during winter (up to $7 \text{ Tg CH}_4 \text{ mon}^{-1}$ during December, January, and February, Figures 2a and 3a).

Table 10*Historical Simulations Compared With Previous Global Wetland Emission Estimates*

Studies	Period	Comments	Emission value (Tg CH ₄ year ⁻¹)
Our study	1950–2012	Bottom-up approach, process-based model considering multiple natural wetland types	185–217
Zhang et al. (2017)	2000–2007	Bottom-up approach, using same model as Tian et al., 2015 but using five different wetland distribution data sets	127–227
Saunois et al. (2016)	2000–2012	Top-down and bottom-up approach, multiple model approaches, natural wetland emissions, and tropical regions are hot spots	125–227
Tian et al. (2015)	1981–2010	Bottom-up approach, land surface emissions considered agriculture, tropical, and Asia are hot spots	131–157
Zhu et al. (2015)	1901–2012	Bottom-up approach, wetland emissions considered agriculture, primarily controlled by tropical wetlands, peak occurring in 1991–2012	209–245
Kirschke et al. (2013)	2000–2009	Top-down and bottom-up approach, multiple model approaches, natural wetland emissions	142–284

data from different sources vary significantly (Figure S4). Wetland inundation area fraction data showed a high peak during summer and a low peak during winter. The M&F data have the biggest global average value (5.2 Mkm² in our model), but the SWAMPS-GLWD data can be higher than M&F data during summer (up to 6.5 Mkm² in our model, Figure S4). The M&F data do not have seasonal variation and provide the same amount of inundated area during winter as in summer without considering soil frozen. TEM-MDM will not stop produce methane when soil temperature is lower than 0°C, and this process will increase the winter estimate when using M&F data to some extent. Using different sets of climate forcing data, the emission estimates using CRU data are lower than using ECMWF and NCEP data (Figure 4). When using different wetland distribution data, the methane emission estimates vary up to 26 Tg CH₄ year⁻¹ (Table 8 and Figure 4). Global distribution of methane emissions and consumptions do not change significantly when using different climate forcing data but will change significantly when using different wetland distribution data (Figures S5 and S6). Global methane emission and consumption changes indicate that SWAMPS-GLWD has smaller wetland inundated area in boreal regions and larger area in tropical regions in comparison to M&F data (Figures S5 and S6).

4.4. Comparison With Other Studies

The previous global estimates of methane emissions from wetlands range from 127 to 284 Tg CH₄ year⁻¹ for various historical periods (Table 10). This study estimates the global methane emissions of 185–217 Tg CH₄ year⁻¹ from wetlands, when using CRU climate data and SWAMPS-GLWD wetland inundation area fraction data (Table 10). For boreal regions, our model showed relatively lower mean emissions (~6 Tg CH₄ year⁻¹, Figure 5c) than previous mean estimates (14–16 Tg CH₄ year⁻¹, Kirschke et al., 2013 ; Saunois et al., 2016). This might be due to wetland inundation area uncertainty, such as inclusion of inland water in Poulter et al. (2017), and due to the lack of long-term methane fluxes observations from higher latitudes (>60°N, Table 1), resulting in methane emissions from boreal regions varying from 1 to 25 Tg CH₄ year⁻¹. For temperate regions, our model showed a large peak and higher emissions (up to 4 Tg CH₄ year⁻¹ degree⁻¹) when comparing with previous studies in latitudinal distributions (Figure 5c, Saunois et al., 2016, Kirschke et al., 2013). This should be due to lack of long-term methane flux observation data from the region close to tropics (30–40°N) in our modeling. Regions including Eastern United States, Middle East, and eastern China showed large emissions during summer, at 29 and 27 Tg CH₄ year⁻¹, respectively, because of high temperature (Figure 5a). Although regional results from previous works (Saunois et al., 2016; Kirschke et al., 2013) also indicated that Eastern United States and eastern China are hotspots, South America should be the biggest source (average ~80 Tg CH₄ year⁻¹, with 40–60% uncertainties). We estimate that methane emissions from South America are lower than previous studies (Saunois et al., 2016, Kirschke et al., 2013). This is mainly due to extremely lack of the observation data from tropical regions and large uncertainties in wetland inundation area identifications (Table 1, Poulter et al., 2017). Besides, Amazon basin observations have recently found that tropical trees act as significant conduits for wetland CH₄ emissions (Pangala et al., 2017). Our current estimates however have not accounted for these effects. In the simulations during 1950–2012, both emission and consumption increased during El Niño events and decreased during La Niña events (Figure 6). Zhu et al. (2017) showed an opposite result, indicating there were less

emissions from tropical regions during El Niño events and more emissions during La Niña events. This discrepancy might be due to that methane emissions and consumptions are more sensitive to air temperature change in our model. During El Niño events, the global mean air temperature would increase so the methane emission and consumption would increase. During La Niña events, global mean temperature is generally relatively low and would decrease methane emission and consumption. Compared to previous modeling studies (Cao et al., 1995, 1996; Li, 2000; Meng et al., 2012; Walter & Heimann, 2000; Zhu et al., 2014; Zhuang et al., 2004), this study considers wetland types in different climatic regions and the influence of standing water for methane emissions. We use a finer time step (1 hr for methane module and 5 min for hydrology module) than before to reduce partial differential equation solution errors.

5. Conclusions

This study quantifies the uncertainty sources and magnitudes of global land methane emissions and consumption. We find that parameters, wetland type distribution, and wetland area distribution are three major uncertainty sources for methane emissions, inducing emission uncertainty 62, 32, and up to 26 Tg CH₄ year⁻¹, respectively. Climate forcing uncertainties result in the emission uncertainty up to 9 Tg CH₄ year⁻¹. Driven with CRU forcing data and SWAMPS-GLWD inundation area fraction data, our model estimates that the global wetlands emit 198 Tg CH₄ year⁻¹ and uplands consume 32 Tg CH₄ year⁻¹ during 1950–2012. Global methane emissions and consumption increase during El Niño events and decrease during La Niña events. Our estimates can be improved by using more in situ data in parameterization and more accurate dynamical wetlands and inundation distribution data to drive our model. This study provided an improved process-based methane biogeochemistry model to the research community and helped identify important uncertainty sources and controlling factors for quantifying global wetland methane emissions. By organizing and using a large field data set of methane fluxes for model parameterization and evaluation, this study helped significantly constrain the global wetland emission uncertainty.

Data Availability Statement

All data used in this manuscript can be accessed in Purdue University Research Repository (PURR) (through the link: <https://doi.org/10.4231/W1M6-4651>).

Acknowledgments

This study is supported by NASA (NNX17AK20G), the Department of Energy (DESC0008092 and DE-SC0007007), and the NSF Division of Information and Intelligent Systems (NSF-1028291). The supercomputing is provided by the Rosen Center for Advanced Computing at Purdue University. We are also grateful to the University of Tuscia (dep. DIBAF), Italy, and their affiliated members for their help and the use of their field data.

References

- Anderson, B., Bartlett, K. B., Frolking, S., Hayhoe, K., Jenkins, J. C., & Salas, W. A. (2010). *Methane and nitrous oxide emissions from natural sources*. Washington DC, USA: Office of Atmospheric Program, US Environmental Protection Agency, EPA 430-R-10-001.
- Arah, J. R. M., & Stephen, K. D. (1998). A model of the processes leading to methane emission from peatland. *Atmospheric Environment*, 32(19), 3257–3264. [https://doi.org/10.1016/S1352-2310\(98\)00052-1](https://doi.org/10.1016/S1352-2310(98)00052-1)
- Arneth, A., Sitch, S., Bondeau, A., Butterbach-Bahl, K., Foster, P., Gedney, N., et al. (2010). From biota to chemistry and climate: Towards a comprehensive description of trace gas exchange between the biosphere and atmosphere. *Biogeosciences*, 7(1), 121–149. <https://doi.org/10.5194/bg-7-121-2010>
- Bartlett, D. S., Bartlett, K. B., Hartman, J. M., Harriss, R. C., Sebacher, D. I., Pelletier-Travis, R., et al. (1989). Methane emissions from the Florida Everglades: Patterns of variability in a regional wetland ecosystem. *Global Biogeochemical Cycles*, 3(4), 363–374. <https://doi.org/10.1029/GB003i004p00363>
- Bartlett, K. B., Crill, P. M., Sebacher, D. I., Harriss, R. C., Wilson, J. O., Melack, J. M. (1988). Methane flux from the central Amazonian floodplain. *Journal of Geophysical Research*, 93, (D2), 1571. <https://doi.org/10.1029/jd093id02p01571>
- Bartlett, K. B., Crill, P. M., Bonnassi, J. A., Richey, J. E., & Harriss, R. C. (1990). Methane flux from the Amazon River floodplain: Emissions during rising water. *Journal of Geophysical Research*, 95(D10), 16,773–16,788. <https://doi.org/10.1029/JD095iD10p16773>
- Belger, L., Forsberg, B. R., & Melack, J. M. (2011). Carbon dioxide and methane emissions from interfluvial wetlands in the upper Negro River basin, Brazil. *Biogeochemistry*, 105(1–3), 171–183. <https://doi.org/10.1007/s10533-010-9536-0>
- Bender, M., & Conrad, R. (1992). Kinetics of CH₄ oxidation in oxic soils exposed to ambient air or high CH₄ mixing ratios. *FEMS Microbiology Letters*, 101(4), 261–270. [https://doi.org/10.1016/0168-6496\(92\)90043-s](https://doi.org/10.1016/0168-6496(92)90043-s)
- Bonan, G. B. (1996). *Land surface model (LSM version 1.0) for ecological, hydrological, and atmospheric studies: Technical description and users guide*. Technical note (no. PB-97-131494/XAB; NCAR/TN-417-STR). National Center for Atmospheric Research, Boulder, CO (United States). Climate and global dynamics div
- Boon, P. I., & Mitchell, A. (1995). Methanogenesis in the sediments of an Australian freshwater wetland: Comparison with aerobic decay, and factors controlling methanogenesis. *FEMS Microbiology Ecology*, 18(3), 175–190. <https://doi.org/10.1111/j.1574-6941.1995.tb00175.x>
- Burke Jr., R. A., Barber, T. R., & Sackett, W. M. (1988). Methane flux and stable hydrogen and carbon isotope composition of sedimentary methane from the Florida Everglades. *Global Biogeochemical Cycles*, 2(4), 329–340. <https://doi.org/10.1029/gb002i004p00329>
- Cao, M., Dent, J. B., & Heal, O. W. (1995). Modeling methane emissions from rice paddies. *Global Biogeochemical Cycles*, 9(2), 183–195. <https://doi.org/10.1029/94GB03231>
- Cao, M., Marshall, S., & Gregson, K. (1996). Global carbon exchange and methane emissions from natural wetlands: Application of a process-based model. *Journal of Geophysical Research*, 101(D9), 14,399–14,414. <https://doi.org/10.1029/96JD00219>

- Chen, H., Zhai, Q. A., Peng, C., Wu, N., Wang, Y., Fang, X., et al. (2013). Methane emissions from rice paddies natural wetlands, lakes in China: Synthesis new estimate. *Global Change Biology*, 19(1), 19–32. <https://doi.org/10.1111/gcb.12034>
- Chen, Y. H., & Prinn, R. G. (2005). Atmospheric modeling of high-and low-frequency methane observations: Importance of interannually varying transport. *Journal of Geophysical Research*, 110, D10303. <https://doi.org/10.1029/2004jd005542>
- Ciais, P., Sabine, C., Bala, G., Bopp, L., Brovkin, V., Canadell, J., & Jones, C. (2013). Carbon and other biogeochemical cycles. Climate change 2013: The physical science basis. In *Contribution of working group I to the fifth assessment report of the intergovernmental panel on climate change*, (pp. 465–570). Cambridge United Kingdom and New York NY USA: Cambridge University Press.
- Clement, R. J., Verma, S. B., & Verry, E. S. (1995). Relating chamber measurements to eddy correlation measurements of methane flux. *Journal of Geophysical Research*, 100(D10), 21,047–21,056. <https://doi.org/10.1029/95JD02196>
- Cui, B. (1997). Estimation of CH₄ emission from Sanjiang plain. *Scientia Geographica Sinica*, 17, 93–95. (in Chinese with English abstract). <http://geosciencenigae.ac.cn/CN/10.13249/j.cnki.sgs.1997.01.93>
- Dee, D. P., Uppala, S. M., Simmons, A. J., Berrisford, P., Poli, P., Kobayashi, S., et al. (2011). The ERA-interim reanalysis: Configuration and performance of the data assimilation system. *Quarterly Journal of the Royal Meteorological Society*, 137(656), 553–597. <https://doi.org/10.1002/qj.828>
- Devol, A. H., Richey, J. E., Clark, W. A., King, S. L., & Martinelli, L. A. (1988). Methane emissions to the troposphere from the Amazon floodplain. *Journal of Geophysical Research*, 93(D2), 1583–1592. <https://doi.org/10.1029/JD093iD02p01583>
- Ding, W., Cai, Z., & Wang, D. (2004). Preliminary budget of methane emissions from natural wetlands in China. *Atmospheric Environment*, 38(5), 751–759. <https://doi.org/10.1016/j.atmosenv.2003.10.016>
- Dise, N. (1993). Methane emission from Minnesota peatlands: Spatial and seasonal variability. *Global Biogeochemical Cycles*, 7(1), 123–142. <https://doi.org/10.1029/92GB02299>
- Drugokencky, E. J., Bruhwiler, L., White, J. W. C., Emmons, L. K., Novelli, P. C., Montzka, S. A., et al. (2009). Observational constraints on recent increases in the atmospheric CH₄ burden. *Geophysical Research Letters*, 36, L18803. <https://doi.org/10.1029/2009GL039780>
- Duan, Q. Y., Gupta, V. K., & Sorooshian, S. (1993). Shuffled Complex Evolution Approach for effective and efficient global minimization. *Journal of Optimization Theory and Applications*, 76(3), 501–521. <https://doi.org/10.1007/BF00939380>
- Etheridge, D. M., Steele, L., Francey, R. J., & Langenfelds, R. L. (1998). Atmospheric methane between 1000 AD and present: Evidence of anthropogenic emissions and climatic variability. *Journal of Geophysical Research*, 103(D13), 15,979–15,993. <https://doi.org/10.1029/98JD00923>
- Glagolev, M., Kleptsova, I., Filippov, I., Maksyutov, S., & Machida, T. (2011). Regional methane emission from West Siberia mire landscapes. *Environmental Research Letters*, 6(4), 045214. <https://doi.org/10.1088/1748-9326/6/4/045214>
- Granberg, G., Ottosson-Löfvenius, M., Grip, H., Sundh, I., & Nilsson, M. (2001). Effect of climatic variability from 1980 to 1997 on simulated methane emission from a boreal mixed mire in northern Sweden. *Global Biogeochemical Cycles*, 15(4), 977–991. <https://doi.org/10.1029/2000GB001356>
- Hao, Q. J., Wang, Y. S., Song, C. C., Liu, G. R., Wang, Y. Y., & Wang, M. X. (2004). Study of CH₄ emission from wetlands in Sanjiang plain. *Journal of Soil and Water Conservation*, 18(3), 194–199. <http://www.cnki.com.cn/Article/CJFD2004-NHBH200405002.htm>
- Harris, I. P. D. J., Jones, P. D., Osborn, T. J., & Lister, D. H. (2014). Updated high-resolution grids of monthly climatic observations—The CRU TS3. 10 dataset. *International Journal of Climatology*, 34(3), 623–642. <https://doi.org/10.1002/joc.3711>
- Harrison, R. C., Sebacher, D. I., Bartlett, K. B., Bartlett, D. S., & Crill, P. M. (1988). Sources of atmospheric methane in the South Florida environment. *Global Biogeochemical Cycles*, 2(3), 231–243. <https://doi.org/10.1029/GB002i003p00231>
- Hodson, E. L., Poulter, B., Zimmermann, N. E., Prigent, C., & Kaplan, J. O. (2011). The El Niño–southern oscillation and wetland methane interannual variability. *Geophysical Research Letters*, 38, L08810. <https://doi.org/10.1029/2011GL046861>
- Hopcroft, P. O., Valdes, P. J., O'Connor, F. M., Kaplan, J. O., & Beerling, D. J. (2017). Understanding the glacial methane cycle. *Nature Communications*, 8(1), 14,383. <https://doi.org/10.1038/ncomms14383>
- Huang, Y. A. O., Sun, W., Zhang, W. E. N., Yu, Y., Su, Y., & Song, C. (2010). Marshland conversion to cropland in Northeast China from 1950 to 2000 reduced the greenhouse effect. *Global Change Biology*, 16(2), 680–695. <https://doi.org/10.1111/j.1365-2486.2009.01976.x>
- Ito, A., & Inatomi, M. (2012). Use of a process-based model for assessing the methane budgets of global terrestrial ecosystems and evaluation of uncertainty. *Biogeosciences*, 9(2), 759–773. <https://doi.org/10.5194/bg-9-759-2012>
- Jackson-Korczyński, M., Christensen, T. R., Bäckstrand, K., Crill, P., Friberg, T., Mastepanov, M., & Ström, L. (2010). Annual cycle of methane emission from a subarctic peatland. *Journal of Geophysical Research*, 115, G02009. <https://doi.org/10.1029/2008JG000913>
- Kalnay, E., Kanamitsu, M., Kistler, R., Collins, W., Deaven, D., Gandin, L., et al. (1996). The NCEP/NCAR 40-year reanalysis project. *Bulletin of the American Meteorological Society*, 77(3), 437–471. [https://doi.org/10.1175/1520-0477\(1996\)077<0437:TNYRP>2.0.CO;2](https://doi.org/10.1175/1520-0477(1996)077<0437:TNYRP>2.0.CO;2)
- Kirschke, S., Bousquet, P., Ciais, P., Saunois, M., Canadell, J. G., Druck, E. J., et al. (2013). Three decades of global methane sources and sinks. *Nature Geoscience*, 6(10), 813–823. <https://doi.org/10.1038/ngeo1955>
- Kleinen, T., Brovkin, V., & Schuldt, R. J. (2012). A dynamic model of wetland extent and peat accumulation: Results for the Holocene. *Biogeosciences*, 9(1), 235–248. <https://doi.org/10.5194/bg-9-235-2012>
- Lehner, B., & Döll, P. (2004). Development and validation of a global database of lakes, reservoirs and wetlands. *Journal of Hydrology*, 296(1–4), 1–22. <https://doi.org/10.1016/j.jhydrol.2004.03.028>
- Li, C. S. (2000). Modeling trace gas emissions from agricultural ecosystems. In *Methane emissions from major rice ecosystems in Asia*, (pp. 259–276). Dordrecht: Springer.
- Liu, L., Zhuang, Q., Zhu, Q., Liu, S., van Asperen, H., & Pihlatie, M. (2018). Global soil consumption of atmospheric carbon monoxide: An analysis using a process-based biogeochemistry model. *Atmospheric Chemistry and Physics (Online)*, 18(11). <https://doi.org/10.5194/acp-18-7913-2018>
- MacFarling Meure, C., Etheridge, D., Trudinger, C., Steele, P., Langenfelds, R., Van Ommen, T., et al. (2006). Law dome CO₂, CH₄ and N₂O ice core records extended to 2000 years BP. *Geophysical Research Letters*, 33, L14810. <https://doi.org/10.1029/2006GL026152>
- Matthews, E., & Fung, I. (1987). Methane emission from natural wetlands: Global distribution, area, and environmental characteristics of sources. *Global Biogeochemical Cycles*, 1(1), 61–86. <https://doi.org/10.1029/GB001i001p00061>
- Melack, J. M., Hess, L. L., Gastil, M., Forsberg, B. R., Hamilton, S. K., Lima, I. B., & Novo, E. M. (2004). Regionalization of methane emissions in the Amazon basin with microwave remote sensing. *Global Change Biology*, 10(5), 530–544. <https://doi.org/10.1111/j.1365-2486.2004.00763.x>
- Melillo, J. M., McGuire, A. D., Kicklighter, D. W., Moore, B., Vorosmarty, C. J., & Schloss, A. L. (1993). Global climate change and terrestrial net primary production. *Nature*, 363(6426), 234–240. <https://doi.org/10.1038/363234a0>

- Melton, J., Wania, R., Hodson, E. L., Poulter, B., Ringeval, B., Spahni, R., et al. (2013). Present state of global wetland extent and wetland methane modelling: Conclusions from a model inter-comparison project (WETCHIMP). *Biogeosciences*, 10, 753–788. <https://doi.org/10.5194/bg-10-753-2013>
- Melton, J. R., & Arora, V. K. (2016). Competition between plant functional types in the Canadian Terrestrial Ecosystem Model (CTEM) v. 2.0. *Geosci. Model Dev.*, 9, 323–361. <https://doi.org/10.5194/gmd-9-323-2016>
- Meng, L., Hess, P. G. M., Mahowald, N. M., Yavitt, J. B., Riley, W. J., Subin, Z. M., et al. (2012). Sensitivity of wetland methane emissions to model assumptions: Application and model testing against site observations. *Biogeosciences*, 9(7), 2793–2819. <https://doi.org/10.5194/bg-9-2793-2012>
- Moore, T. R., De Young, A., Bubier, J. L., Humphreys, E. R., Lafleur, P. M., & Roulet, N. T. (2011). A multi-year record of methane flux at the Mer Bleue bog, southern Canada. *Ecosystems*, 14(4), 646–657. <https://doi.org/10.1007/s10021-011-9435-9>
- Nahlik, A. M., & Mitsch, W. J. (2011). Methane emissions from tropical freshwater wetlands located in different climatic zones of Costa Rica. *Global Change Biology*, 17(3), 1321–1334. <https://doi.org/10.1111/j.1365-2486.2010.02190.x>
- Nisbet, E. G., Dlugokencky, E. J., & Bousquet, P. (2014). Methane on the rise—Again. *Science*, 343(6170), 493–495. <https://doi.org/10.1126/science.1247828>
- Pangala, S. R., Enrich-Prast, A., Basso, L. S., Peixoto, R. B., Bastviken, D., Hornbrook, E. R., et al. (2017). Large emissions from floodplain trees close to the Amazon methane budget. *Nature*, 552(7684), 230–234. <https://doi.org/10.1038/nature24639>
- Pelletier, L., Moore, T. R., Roulet, N. T., Garneau, M., & Beaulieu-Audy, V. (2007). Methane fluxes from three peatlands in the La Grande Rivière watershed, James Bay lowland, Canada. *Journal of Geophysical Research*, 112. <https://doi.org/10.1029/2006JG000216>
- Petrescu, A. M. R., Van Beek, L. P. H., Van Huissteden, J., Prigent, C., Sachs, T., Corradi, C. A. R., et al. (2010). Modeling regional to global CH₄ emissions of boreal and arctic wetlands. *Global Biogeochemical Cycles*, 24, GB4009. <https://doi.org/10.1029/2009GB003610>
- Poulter, B., Bousquet, P., Canadell, J. G., Ciais, P., Peregon, A., Saunois, M., et al. (2017). Global wetland contribution to 2000–2012 atmospheric methane growth rate dynamics. *Environmental Research Letters*, 12(9), 094013. <https://doi.org/10.1088/1748-9326/aa8391>
- Quiquet, A., Archibald, A. T., Friend, A. D., Chappellaz, J., Levine, J. G., Stone, E. J., et al. (2015). The relative importance of methane sources and sinks over the last interglacial period and into the last glaciation. *Quaternary Science Reviews*, 112, 1–16. <https://doi.org/10.1016/j.quascirev.2015.01.004>
- Riley, W. J., Subin, Z. M., Lawrence, D. M., Swenson, S. C., Torn, M. S., Meng, L., et al. (2011). Barriers to predicting changes in global terrestrial methane fluxes: Analyses using CLM4Me, a methane biogeochemistry model integrated in CESM. *Biogeosciences*, 8(7), 1925–1953. <https://doi.org/10.5194/bg-8-1925-2011>
- Ringeval, B., Friedlingstein, P., Koven, C., Ciais, P., de Noblet-Ducoudré, N., Decharme, B., & Cadule, P. (2010). Climate-CH₄ feedback from wetlands and its interaction with the climate-CO₂ feedback. *Biogeosciences*, 8(8), 2137–2157. <https://doi.org/10.5194/bg-8-2137-2011>
- Rinne, J., Riutta, T., Pihlatie, M., Aurela, M., Haapanala, S., Tuovinen, J. P., et al. (2007). Annual cycle of methane emission from a boreal fen measured by the eddy covariance technique. *Tellus B: Chemical and Physical Meteorology*, 59(3), 449–457. <https://doi.org/10.1111/j.1600-0889.2007.00261.x>
- Saarnio, S., Alm, J., Silvola, J., Lohila, A., Nykänen, H., & Martikainen, P. J. (1997). Seasonal variation in CH₄ emissions and production and oxidation potentials at microsites on an oligotrophic pine fen. *Oecologia*, 110(3), 414–422. <https://doi.org/10.1007/s004420050176>
- Saunois, M., Bousquet, P., Poulter, B., Peregon, A., Ciais, P., Canadell, J. G., & Janssens-Maenhout, G. (2016). The global methane budget 2000–2012. *Earth System Science Data*, 8(2), 697–751. <https://doi.org/10.5194/essd-8-697-2016>
- Saunois, M., Stavert, A. R., Poulter, B., Bousquet, P., Canadell, J. G., Jackson, R. B., & Dlugokencky, E. J. (2019). The global methane budget 2000–2017. *Earth System Science Data Discussion*. <https://www.earth-syst-sci-data-discuss.net/essd-2019-128/>
- Schaefer, H., Fletcher, S. E. M., Veidt, C., Lassey, K. R., Brailsford, G. W., Bromley, T. M., et al. (2016). A 21st-century shift from fossil-fuel to biogenic methane emissions indicated by ¹³CH₄. *Science*, 352(6281), 80–84. <https://doi.org/10.1126/science.aad2705>
- Schroeder, R., McDonald, K., Chapman, B., Jensen, K., Podest, E., Tessler, Z., et al. (2015). Development and evaluation of a multi-year fractional surface water data set derived from active/pассив microwave remote sensing data. *Remote Sensing*, 7(12), 16,688–16,732. <https://doi.org/10.3390/rs71215843>
- Sellers, P. J., Hall, F. G., Kelly, R. D., Black, A., Baldocchi, D., Berry, J., et al. (1997). BOREAS in 1997: Experiment overview, scientific results, and future directions. *Journal of Geophysical Research*, 102(D24), 28,731–28,769. <https://doi.org/10.1029/97JD03300>
- Shannon, R. D., & White, J. R. (1994). A three-year study of controls on methane emissions from two Michigan peatlands. *Biogeochemistry*, 27(1), 35–60. <https://doi.org/10.1007/bf00002570>
- Shurpali, N. J., & Verma, S. B. (1998). Micrometeorological measurements of methane flux in a Minnesota peatland during two growing seasons. *Biogeochemistry*, 40(1), 1–15. <https://doi.org/10.1023/A:1005875307146>
- Shurpali, N. J., Verma, S. B., Clement, R. J., & Billesbach, D. P. (1993). Seasonal distribution of methane flux in a Minnesota peatland measured by eddy correlation. *Journal of Geophysical Research*, 98(D11), 20,649–20,655. <https://doi.org/10.1029/93JD02181>
- Song, C., Xu, X., Tian, H., & Wang, Y. (2009). Ecosystem–atmosphere exchange of CH₄ and N₂O and ecosystem respiration in wetlands in the Sanjiang plain, northeastern China. *Global Change Biology*, 15(3), 692–705. <https://doi.org/10.1111/j.1365-2486.2008.01821.x>
- Spahni, R., Wania, R., van Velthoven, P., Neef, L., van Wheele, M., Pison, I., et al. (2011). Constraining global methane emissions and uptake by ecosystems. *Biogeosciences*, 8(6), 1643–1665. <https://doi.org/10.5194/bg-8-1643-2011>
- Svensson, B. H., Christensen, T. R., Johansson, E., & Öquist, M. (1999). Interdecadal changes in CO₂ and CH₄ fluxes of a subarctic mire: Stordalen revisited after 20 years. *Oikos*, 85, 22–30. <https://doi.org/10.2307/3546788>
- Tang, J., Zhuang, Q., Shannon, R. D., & White, J. R. (2010). Quantifying wetland methane emissions with process-based models of different complexities. *Biogeosciences*, 7(11), 3817–3837. <https://doi.org/10.5194/bg-7-3817-2010>
- Tian, H., Chen, G., Lu, C., Xu, X., Ren, W., Zhang, B., et al. (2015). Global methane and nitrous oxide emissions from terrestrial ecosystems due to multiple environmental changes. *Ecosystem Health and Sustainability*, 1(1), 1–20. <https://doi.org/10.1890/EHS14-0015.1>
- Tian, H., Xu, X., Liu, M., Ren, W., Zhang, C., Chen, G., & Lu, C. (2010). Spatial and temporal patterns of CH₄ and N₂O fluxes in terrestrial ecosystems of North America during 1979–2008: Application of a global biogeochemistry model. *Biogeosciences*, 7(9), 2673–2694. <https://doi.org/10.5194/bg-7-2673-2010>
- Van Huissteden, J., van den Bos, R., & Alvarez, I. M. (2006). Modelling the effect of water-table management on CO₂ and CH₄ fluxes from peat soils. *Netherlands Journal of Geosciences*, 85(1), 3–18. <https://doi.org/10.1017/S0016774600021399>
- Walter, B. P., & Heimann, M. (2000). A process-based, climate-sensitive model to derive methane emissions from natural wetlands: Application to five wetland sites, sensitivity to model parameters, and climate. *Global Biogeochemical Cycles*, 14(3), 745–765. <https://doi.org/10.1029/1999GB001204>

- Walter, B. P., Heimann, M., & Matthews, E. (2001a). Modeling modern methane emissions from natural wetlands: 1. Model description and results. *Journal of Geophysical Research*, 106(D24), 34,189–34,206. <https://doi.org/10.1029/2001JD900165>
- Walter, B. P., Heimann, M., & Matthews, E. (2001b). Modeling modern methane emissions from natural wetlands: 2. Interannual variations 1982–1993. *Journal of Geophysical Research*, 106(D24), 34,207–34,219. <https://doi.org/10.1029/2001JD900164>
- Wang, D. X., Lu, X. G., Ding, W. X., Cai, Z. C., & Wang, Y. Y. (2002). Comparison of methane emission from marsh and paddy field in Sanjiang plain. *Scientia Geographica Sinica*, 22(4), 500–503. <http://geoscien.neigae.ac.cn/CN/10.13249/j.cnki.sgs.2002.04.500> (in Chinese with English abstract)
- Wania, R., Ross, I., & Prentice, I. C. (2010). Implementation and evaluation of a new methane model within a dynamic global vegetation model: LPJ-WHyMe v1. 3.1. *Geoscientific Model Development*, 3(2), 565–584. <https://doi.org/10.5194/gmd-3-565-2010>
- Wickland, K. P., Striegl, R. G., Mast, M. A., & Clow, D. W. (2001). Interannual variation of soil respiration in two New England forests. *Global Biogeochemistry Cycle*, 15, 321. <https://doi.org/10.1029/2000gb001325>
- Woodward, F. I., & Lomas, M. R. (2004). Vegetation dynamics—simulating responses to climatic change. *Biological Reviews*, 79(3), 643–670. <https://doi.org/10.1017/S1464793103006419>
- Xu, X., Riley, W. J., Koven, C. D., Billesbach, D. P., Chang, R. Y. W., Commane, R., et al. (2016). A multi-scale comparison of modeled and observed seasonal methane emissions in northern wetlands. *Biogeosciences (Online)*, 13(17). <https://doi.org/10.5194/bg-13-5043-2016>
- Yang, J. S., Liu, J. S., Wang, J. D., Yu, J. B., Sun, Z. G., & Li, X. H. (2006). Emissions of CH₄ and N₂O from a wetland in the Sanjiang plain. *Journal of Plant Ecology*, 30(3), 432–440. <https://doi.org/10.17521/cjpe.2006.0058>
- Zhang, Y., Li, C., Trettin, C. C., Li, H., & Sun, G. (2002). An integrated model of soil, hydrology, and vegetation for carbon dynamics in wetland ecosystems. *Global Biogeochemical Cycles*, 16(4), 9–1. <https://doi.org/10.1029/2001gb001838>
- Zhang, Z., Zimmermann, N. E., Calle, L., Hurt, G., Chatterjee, A., & Poulet, B. (2018). Enhanced response of global wetland methane emissions to the 2015–2016 El Niño-southern oscillation event. *Environmental Research Letters*, 13(7), 074009. <https://doi.org/10.1088/1748-9326/aac939>
- Zhang, Z., Zimmermann, N. E., Stenke, A., Li, X., Hodson, E. L., Zhu, G., et al. (2017). Emerging role of wetland methane emissions in driving 21st century climate change. *Proceedings of the National Academy of Sciences*, 114(36), 9647–9652. <https://doi.org/10.1073/pnas.1618765114>
- Zhu, Q., Liu, J., Peng, C., Chen, H., Fang, X., Jiang, H., et al. (2014). Modelling methane emissions from natural wetlands by development and application of the TRIPLEX-GHG model. *Geoscientific Model Development*, 7(3), 981–999. <https://doi.org/10.5194/gmd-7-981-2014>
- Zhu, Q., Peng, C., Chen, H., Fang, X., Liu, J., Jiang, H., et al. (2015). Estimating global natural wetland methane emissions using process modelling: Spatio-temporal patterns and contributions to atmospheric methane fluctuations. *Global Ecology and Biogeography*, 24(8), 959–972. <https://doi.org/10.1111/geb.12307>
- Zhu, Q., Peng, C., Ciais, P., Jiang, H., Liu, J., Bousquet, P., et al. (2017). Interannual variation in methane emissions from tropical wetlands triggered by repeated El Niño southern oscillation. *Global Change Biology*, 23(11), 4706–4716. <https://doi.org/10.1111/gcb.13726>
- Zhuang, Q., Chen, M., Xu, K., Tang, J., Saikawa, E., Lu, Y., et al. (2013). Response of global soil consumption of atmospheric methane to changes in atmospheric climate and nitrogen deposition. *Global Biogeochemical Cycles*, 27, 650–663. <https://doi.org/10.1002/gbc.20057>
- Zhuang, Q., & Crill, P. (2008). NCEAS 10645: Toward an adequate quantification of CH₄ emissions from land ecosystems: Integrating field and in-situ observations, satellite data, and modeling. In *Sallies fen NH CH₄ flux 1994–2001*. SE-106 91 Stockholm, Sweden: National Center for Ecological analysis and synthesis and Stockholm University. <https://knb.ecoinformatics.org/view/doi:10.5063/AA/nceas.890.4>
- Zhuang, Q., McGuire, A. D., Melillo, J. M., Clein, J. S., Dargaville, R. J., Kicklighter, D. W., et al. (2003). Carbon cycling in extratropical terrestrial ecosystems of the Northern Hemisphere during the 20th century: A modeling analysis of the influences of soil thermal dynamics. *Tellus B: Chemical and Physical Meteorology*, 55(3), 751–776. <https://doi.org/10.1034/j1600-0889.2003.00060.x>
- Zhuang, Q., Melillo, J. M., Kicklighter, D. W., Prinn, R. G., McGuire, A. D., Steudler, P. A., et al. (2004). Methane fluxes between terrestrial ecosystems and the atmosphere at northern high latitudes during the past century: A retrospective analysis with a process-based biogeochemistry model. *Global Biogeochemical Cycles*, 18, GB3010. <https://doi.org/10.1029/2004GB002239>
- Zhuang, Q., Melillo, J. M., McGuire, A. D., Kicklighter, D. W., Prinn, R. G., Steudler, P. A., et al. (2007). Net emissions of CH₄ and CO₂ in Alaska: Implications for the region's greenhouse gas budget. *Ecological Applications*, 17(1), 203–212. [https://doi.org/10.1890/1051-0761\(2007\)017\[0203:NEOCAC\]2.0.CO;2](https://doi.org/10.1890/1051-0761(2007)017[0203:NEOCAC]2.0.CO;2)